UNIVERSITY OF GHANA
COLLEGE OF BASIC AND APPLIED SCIENCES

A STUDY TO COMPARE THE MOTORISED WEDGE OUTPUT FACTOR OF AN ELEKTA SYNERGY LINEAR ACCELERATOR WITH REFERENCE DATA (TPS DATA).

BY

AKOSAH KINGSLEY

(10507858)

THIS THESIS/DISSERTATION IS SUBMITTED TO THE UNIVERSITY OF GHANA, LEGON IN PARTIAL FULFILMENT OF THE REQUIREMENT FOR THE AWARD OF MASTER OF PHILOSOPHY (MPHIL) MEDICAL PHYSICS DEGREE.

DEPARTMENT OF MEDICAL PHYSICS,

SCHOOL OF NUCLEAR AND ALLIED SCIENCES

JULY, 2016

DECLARATION

This thesis is the result of research work undertaken by Kingsley Akosah in the Department of Medical Physics, School of Nuclear and Allied Sciences, University of Ghana, under the supervision of Prof. J. H. Amuasi, Dr. Stephen Inkoom and Mr. Samuel Nii Adu Tagoe.

…… Date: ……..

KINGSLEY AKOSAH

(STUDENT)

…….. Date: ……..

PROF. J. H. AMUASI

(CO-SUPERVISOR)

…… Date: ……

DR. STEPHEN INKOOM

(CO-SUPERVISOR)

……. Date: ……....

MR. SAMUEL NII ADU TAGOE

(PRINCIPAL SUPERVISOR)

ABSTRACT

For external beam radiotherapy treatments, high doses are delivered to the cancerous cell. Accuracy and precision of dose delivery are primary requirements for effective and efficient cancer treatment. The dose delivered to the patient might not be uniform and therefore need to be compensated for. In treatment these inhomogeneities are taken care of by using wedge filters and incorporating wedge factors in the Treatment Planning System. Computer controlled wedges were alternatives introduced by different manufacturers of which Motorized wedges (MW) is one of them. The MW was introduced by ELEKTA and this helps to overcome some of the shortcomings of physical wedges. The objectives of this study were to measure MW output factors for 6 MV and 15 MV photon energies for an ELEKTA Synergy. Secondly, to compare the results of MWOF obtained to that of the treatment planning system data. The Motorized Wedge Output Factors (MWOF) were measured for the ELEKTA Synergy for both 6 MV and 15 MV photon energies. With the help of PMMA solid water slabs phantom, the Elekta synergy, thermometer, barometer, PTW farmer type ionization chamber 30010 charges were collected at 100 cm source to surface distance for various square field sizes from 5x5 cm to 30x30 cm and depth of 1.5 cm and 2.5 cm for 6 MV and 15 MV photon energies. Comparing the results with the TPS data, an excellent agreement was found for 6 MV MWOF, with the percentage differences ranging from 0.03% to 1.50%, with a mean of 0.03%. The coefficient of variation of MWOF ranged from 0.023% to 1.07% and 0.001% to 12.89% for the two beams (6 MV and 15 MV) respectively. The relative differences between the calculated and the measured MWOFs increases with field size. In conclusion, there was general agreement between the calculated and measured MWOFs. The consistency of values provide further support that a

standard dataset of photon and electron dosimetry could be established as a guide for future commissioning, beam modeling, and quality assurance purposes.

DEDICATION

This work is dedicated to my parents, Mr. Michael Kwame Attah and Mrs. Mercy Oppong Nyantakyi, my lovely sisters Josephine Attah Darko, Millicent Attah Arhin for having provided me with such rich education and fulfilling my spiritual needs through their immense support, encouragement, love, care and prayers and to Maame Ama Pokuaa for her love, dedication and prayers. To my lecturers and colleagues.

ACKNOWLEDGEMENT

Unto the King eternal, invisible, the only wise GOD be praise, honour and glory from time everlasting.

I would like to express my utmost gratitude and appreciation to my supervisors Prof. J. H. Amuasi, Dr. Stephen Inkoom, and Mr. Samuel Nii Tagoe for their immeasurable and valuable contributions, guidance, patience, encouragement and suggestions in the preparation of this thesis.

Again my sincere thanks also goes to Prof A. K. Kyere (Head of Department, Graduate School of Nuclear and allied Science, Medical Physics Department) for his huge guidance, encouragement and immense support rendered to me.

I am also grateful to Mr. George Felix Acquah and Mr. Philip Oppong (Medical Physicists and Radiation Protection Officers at Sweden Ghana Medical Centre), Accra for their time and support and for making their facilities available for this research work.

TABLE OF CONTENTS

LIST OF FIGURES

LIST OF TABLES

ABBREVIATIONS

2D-XRT	Two Dimensional X-ray Radiotherapy
3D	Three Dimensional
3D-CRT	Three Dimensional Conformal Radiation Therapy
AAPM	American Association of Physicist in Medicine
ANOVA	Analysis of Variance
ARPANSA	Australian Radiation Protection and Nuclear Safety Agency
BSF	Back Scatter Factor
BJR	British Journal of Radiology
CAL.	Calculated
CCU	Common Control Unit
CEBR	Conventional External Beam Radiotherapy
CNS	Central Nervous System
Co-60	Cobalt-60
CRT	Conformal Radiation Therapy
CT	Computer Tomography
COV (CV)	Coefficient of Variation
DICOM	Digital Imaging and Communications in Medicine
Dmax (Zmax or Xmax)	Depth of Maximum Dose
EBT	External Beam Radiotherapy
ESTRO	European Society for Radiology and Oncology
FFF	Flattening Free-Filter
FS	Field Size

HVL	Halve-Value Layer
IAEA	International Atomic Energy Agency
IBA	Ion Beam Application
ICRU	International Commission on Radiation Units and measurements'
ICF	Insertion Correction Factor
IEC	International Electro Technical Commission
IGRT	Image Guided Radiation Therapy
IMRT	Intensity Modulated Radiotherapy
ISF	Inverse Square Factor
keV	Kilo Electron Volt
LINAC	Linear Accelerator
LC	Liquid Crystal
MCU	Main Control Unit
MC	Monte Carlo
MEA.	Measured
MLC	Multileaf Collimator
MRI	Magnetic Resonance Imaging
MU	Monitor Unit
MV	Mega Voltage
MeV	Mega Electron Volt
MWOF	Motorized Wedge Output Factor
NCR	National Research Council

NCRNM	National Centre for Radiotherapy and Nuclear Medicine
NPL	National Physical Laboratory
PDD	Percentage Depth Dose
PET	Positron Emission Tomography
PMMA	
PSF	Peak Scatter Factor
PSI	Pacific Semiconductors Industries
PTW	Physikalisch-Technische Werkstatten
RA	Regulatory Authority
RD	Relative Difference
RDF	Relative Dose Factor
RF	Radio-Frequency
RFA	Radiation Field Analyzer
SABR	Stereotactic Ablative Radiotherapy
SAD	Source to Axis Distance
SBRT	Stereotactic Body Radiation Therapy
SF	Scatter Factor
SGMC	Sweden Ghana Medical Centre
SRS	Stereotactic Radiosurgery
SSD	Source to Surface Distance
SSDL	Secondary Standard Dosimetry Laboratory
TBI	Total Body Irradiation
TBq	Tera Becquerel
TPS	Treatment Planning System

TPR	Tissue Phantom Ratio
TRS	Technical Report Series
VMAT	Volumetric-Modulated Arc Therapy
WF	Wedge Factor
WHO	World Health Organization
ΓAKR	Air Kerma Rate Constant

CHAPTER ONE

1.0 INTRODUCTION

1.1 Background

Radiotherapy is an irreplaceable part of cancer treatment that makes use of the effects of ionizing radiation on malignant cells. It has the aim of delivering the required high dose to the target volume whilst minimizing the amount of radiation being delivered to normal (healthy) tissues [53]. The radiation comes from a treatment machine outside the body (external-beam radiation therapy) and this is focused on the cancer (target region), or it may come from a radioactive material placed in the body close to the cancer cells (internal radiation therapy or brachytherapy). Systemic radiation therapy makes use of radioactive substances, such as radioactive iodine, that travel in the blood to kill cancer cells. About half of all cancer patients receive some type of radiation therapy sometime during the course of their treatment.

External beam radiotherapy is the most widely used type of radiation therapy, which often uses photon beams. It's a lot like getting an x-ray, but for longer time. This type of radiation is mostly given by linear accelerators (linacs). External beam radiation can be used to treat large areas of the body. It is also used to treat more than one area, such as the main tumor and nearby lymph nodes. External radiation is given daily over several weeks. The radiation is aimed at the cancer, but in most cases it affects the normal tissues surrounding the cancerous cells as it passes through on its way into and out of the body. Intensity modulated proton therapy works in a more different way.

In clinical practice, numerous techniques of irradiation, different tools such as wedge filters and method are used to shape irradiation field and to modulate the intensity of radiation. Dose uniformity or homogeneous dose distribution in the target volume is attained using wedge filters. Wedge filters may be used to even out the isodose surfaces for photon beams striking relatively flat patient surfaces under an oblique beam incidence. The wedge has two sides and they are the thick end called the heel; this is the point where the dose is lowest and the toe. These wedges supplied by teletherapy units or machines manufacturers are made from dense materials such as lead, steel, brass of standard wedge angles 15°, 30°, 45° and 60° whose designs are based on some recommendations [37] and are used as missing tissue compensators or wedge pairs which alters the shape of isodose curves.

1.2 Statement of the Problem

The delivery of accurate radiation dose to patients is of primary concern in radiotherapy since this can cause damage to healthy tissues. This calls for good treatment planning. Wedges form integral part of radiation therapy treatment planning and are a well-established method for dose inhomogeneity compensation. These wedges have number of problems associated with them. As a result of this an alternative was proposed whereby the wedge effect can be implemented by computer-controlled movement of one of the collimator jaws (the Y jaw) and variation in output rate during treatment. This implementation was named differently by each of three different manufacturers: virtual, electronic, and dynamic (Siemens, Elekta, and Varian, respectively). Linear accelerator (Linac) characterization, in terms of percentage dose, output factors, and wedge output

factors, is critical for accurate treatment planning for precise dose delivery during treatment. Monitor units and complete dose distributions are nowadays usually computed with treatment planning systems. The dose calculation algorithms and the dose computation procedures in such systems are often not completely known to the user. The accuracy in these computations must be tested by the local physics staff by performing dose and wedge output factor measurements in phantoms for typical irradiation geometries. The measured MWOFs and that of the TPS data have been found to be in agreement for both 6 and 15 megavoltage energy beams. The purpose of this thesis is to compare the MWOF obtained experimentally and those calculated from TPS data for 6 MV and 15 MV beams from Elekta Synergy Platform linear accelerator.

1.3 Objectives

The main objective of the thesis is to measure the wedge output factor of the Elekta linear accelerator and compare the wedge output factors with reference data (TPS data).

The specific objectives of this research include:

- The determination of absorbed dose to the phantom at x_{max} with various wedges in place.
- The determination of absorbed dose to the phantom at x_{max} without wedges.

1.4 Justification and Relevance of the Study

The treatment of patients using radiotherapy may involve uncertainties (such as, wrong calibration of radiation equipment, misinterpretation of results, patient movements, and

miscalculation of dosimetric quantities) which can lead to severe complications. For this reason, dose must be delivered with the greatest accuracy. Accurate dose delivery in radiation therapy is also achieved when good treatment planning is done. Linac characterization, in terms of percentage depth dose, output factors and wedge output factors is of great essence for accurate treatment planning. . Moreover, a small error in the WOF can run through the treatment planning system (TPS) and create systematic error in all the treatments that may be planned with the treatment planning system. This study takes into consideration, wedge output factor determination of a motorized wedged linac synergy. The study is useful as the results obtained were compared to reference data (TPS data). In other words, it would confirm the data given by the manufacturer, the Treatment Planning System data and in turn acts as a guide when other linacs are to be installed by health institutions.

1.5 Scope of Study

The aim of this study was to determine the wedge output factors of a motorized ELEKTA SYNERGY linac and compare the results with a reference data (TPS data). The study was carried out at the premises of the Sweden Ghana Medical Centre. In determining the wedge output factors, the absorbed dose when the wedge was in place and open fields was measured. This research work was limited to 6 MV and 15 MV since these are the only highest megavoltage beams available in the country at the time of conducting this research work. Data was taken at SGMC because it is the only oncology centre that uses energy beams with motorized wedge for external beam radiotherapy.

CHAPTER TWO

2.0 LITERATURE REVIEW

2.1 Introduction

This chapter discusses relevant literature on the thesis. These include wedge filters, Physical Wedge, Motorized Wedge, Linac Generations, External Beam Radiation Therapy, Gamma Ray Beams and Gamma Ray Units, Basic properties of gamma rays, Physical properties of cobalt-60, Teletherapy source housing, and Dose delivery with teletherapy machines

The use of more than one radiation beam in external photon beam radiotherapy helps achieve a uniform dose distribution inside the target volume with healthy tissues surrounding the target receiving as low as possible a dose. The target dose uniformity as recommended by the ICRU® report 50 falls within +7% and -5% of dose delivered to a well-defined prescription point in the target [48]. Modern photon beam radiotherapy is carried out with a variety of beam energies and field sizes under one of two setup conventions: constant source-surface distance (SSD) for all beams or isocentric setup with a constant source-axis distance (SAD).

In an SSD setup, the distance from the source to the surface of the patient is kept constant for all beams, while for an SAD setup the center of the target volume is placed at the machine isocenter.

Clinical photon beam energies range from superficial (30 kVp to 80 kVp) through orthovoltage (100 kVp to 300 kVp) to megavoltage energies (Co-60 to 25 MV).

Field sizes range from small circular fields used in radiosurgery through standard rectangular and irregular fields to very large fields used for total body irradiations.

High energy beams makes use of wedged fields for isodose distribution modification by compensating dose inhomogeneity in radiotherapy treatments [30]. Wedge angle refers to the angle through which the isodose curves are tilted relative to their nominal position perpendicular to the beam axis at reference depth. The reference depth per the International Commission on Radiation Units and Measurements (ICRU) is 10 cm [9].

Physical wedges are integral part of radiation therapy treatment planning and are a well-established method for dose inhomogeneity compensation. Physical wedges themselves come with well-known problems. Firstly, physical wedges are designed for a limited field size and wedge angle with only four physical wedge angles of 15°, 30°, 45°, and 60° been implemented by all manufacturers. Secondly, the wedge factor is dependent on many variables including beam energy, field size, depth of measurement, and type of accelerator. This is as a result of beam degradation by the physical wedge. These problems can cause dosimetric issues in treatment planning, and also any occasional misalignment of the wedge can produce significant dosimetric error in treatment delivery [32].

Lastly, physical wedges are heavy and cumbersome to use clinically for the therapists (usually must be lifted overhead) and also they present a safety concern for the patient.

To resolve these issues with physical wedges, an alternative, was proposed whereby the wedge effect can be implemented by computer-controlled movement of one of the collimator jaws (the Y jaw) and variation in output rate during treatment [6]. This

implementation was given a different name by each of three different manufacturers: virtual, electronic, and dynamic (Siemens, Elekta, and Varian, respectively). Descriptions of these computer-controlled wedges have been provided in the literature [1]. They have the potential for any arbitrary wedge angle and fixed dimension, instead of the traditional four wedge angles with limited field sizes.

2.2 Wedge Filters

Wedge filters may be used to even out the isodose surfaces for photon beams striking relatively flat patient surfaces under an oblique beam incidence. The wedge has two sides and they are the thick end called the heel; this is the point where the dose is lowest and the end the toe. These wedges supplied by teletherapy units or machines manufacturers are made from dense materials such as lead, steel, brass of standard wedge angles 15°, 30°, 45° and 60° whose designs are based on some recommendations [36]. These can be used as missing tissue compensators or wedge pairs to alter the shape of isodose curves so that two beams can be angled with a small hinge angle at a target volume thereby creating no hotspot. The wedge angle is the angle through which the isodose curves are tilted, relative to their normal position perpendicular to the beam axis at reference depth. The reference depth per the International Commission on Radiation Units and Measurements (ICRU) is 10 cm [9]. Wedge filters decrease the intensity of the beam and must be considered in treatment dose calculations. This change in the beam is characterized by relative isodose distribution and a wedge factor [35].

Wedges are categorized into two. Namely, physical and computer controlled wedges. Computer controlled wedges are also in three categories by virtue of the manufacturers.

They are virtual, dynamic and electronic (motorized) by Siemens, Varian and Elekta respectively.

2.2.1 Physical Wedge

A physical or external wedge is an angled piece of lead or steel that is placed in the beam to produce a gradient in radiation intensity. Placing the physical wedges on the treatment unit's collimator assembly requires manual intervention.

2.2.2 Motorized Wedge

A motorized or internal wedge is a similar device, a physical wedge integrated into the head of the unit and controlled remotely. It is also referred to as the universal wedge. MW is a single physical wedge (60°) which could generate desired angle (0° to 60°) with the combination of open and wedged beam. In the motorized wedge filter technique, a desired wedged beam profile (typically up to 60° wedge angle) is generated by combining the wedged and open beam in the right proportions. The motorized wedge filter has numerous advantages, some of which are no probability of physical injury to operators and patient, handling of physical wedges is not necessary, making wedge selection faster and easier, which results in higher patients throughput and less fatigue for operators and flexibility to generate arbitrary wedge angle instead of the limited standard wedge angles.

2.3 Linac Generations

During the past 40 years, medical linacs have gone through five distinct generations, making the contemporary machines extremely sophisticated in comparison with the machines of the 1960s. Each generation introduced the following new features:

- Low energy photons (4–8 MV): straight-through beam; fixed flattening filter; external wedges; symmetric jaws; single transmission ionization chamber; isocentric mounting.
- Medium energy photons (10–15 MV) and electrons: bent beam; movable target and flattening filter; scattering foils; dual transmission ionization chamber; electron cones.
- High energy photons (18–25 MV) and electrons: dual photon energy and multiple electron energies; achromatic bending magnet; dual scattering foils or scanned electron pencil beam; motorized wedge; asymmetric or independent collimator jaws.
- High energy photons and electrons: computer-controlled operation; dynamic wedge; electronic portal imaging device; multileaf collimator.
- High energy photons and electrons: photon beam intensity modulation with multileaf collimator; full dynamic conformal dose delivery with intensity modulated beams produced with a multileaf collimator; on-board imaging for use in adaptive radiotherapy.

2.3.1 Components of Modern Linacs

The linacs are usually mounted isocentrically and the operational systems are distributed over five major and distinct sections of the machine:

- Gantry;
- Gantry stand or support;
- Modulator cabinet;

- Patient support assembly, i.e., treatment couch;
- Control console.

Also shown are the connections and relationships among the various linac components, listed above. The diagram provides a general layout of linac components; however, there are significant variations from one commercial machine to another, depending on the final electron beam kinetic energy as well as on the particular design used by the manufacturer. The length of the accelerating waveguide depends on the final electron kinetic energy, and ranges from~30 cm at 4 MeV to~150 cm at 25 MeV.

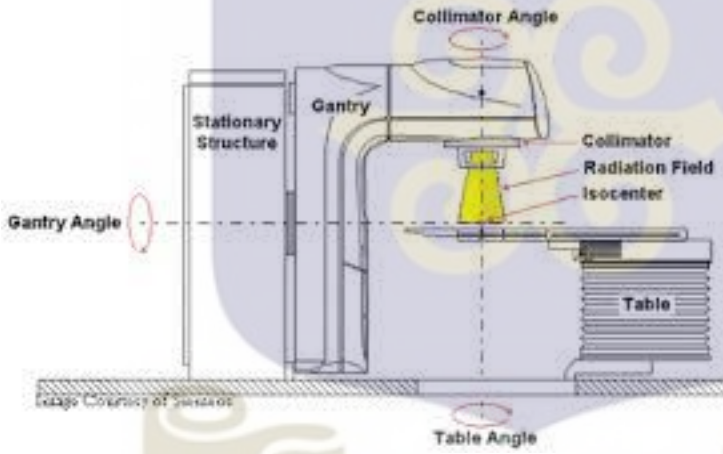

Fig 2.1 A block diagram of Linear Accelerator

The beam-forming components of medical linacs are usually grouped into six classes:

- Injection system;
- RF power generation system;
- Accelerating waveguide;

- Auxiliary system;
- Beam transport system; and
- Beam monitoring system and beam collimation.

The injection system is the source of electrons, essentially a simple electrostatic accelerator called an electron gun. Two types of electron gun are in use: diode type and triode type, both containing a heated cathode (at a negative potential of the order of −25 kV) and a perforated grounded anode. In addition, triode type gun also incorporates a grid placed between the cathode and the anode. Electrons are thermionically emitted from the heated cathode, focused into a pencil beam and accelerated toward the perforated anode through which they drift into the accelerating waveguide. The radiofrequency (RF) power generating system produces the high power microwave radiation used for electron acceleration in the accelerating waveguide and consists of two components: the RF power source and the pulsed modulator. The RF power source is either a magnetron or a klystron in conjunction with a low power RF oscillator. Both devices use electron acceleration and deceleration in vacuum for production of the high power RF fields. The pulsed modulator produces the high voltage, high current, short duration pulses required by the RF power source and the electron injection system. Electrons are accelerated in the accelerating waveguide by means of an energy transfer from the high power RF field which is setup in the accelerating waveguide and produced by the RF power generator. The accelerating waveguide is in principle obtained from a cylindrical uniform waveguide by adding a series of disks (irises) with circular holes at the center, positioned at equal intervals along the tube. These disks separate the waveguide into a series of cylindrical cavities that form the basic structure of the accelerating waveguide in a linac.

The auxiliary system of a linac comprises of several basic systems that are not directly involved with electron acceleration, yet they make the acceleration possible and the linac viable for clinical operation. These systems are: the vacuum-pumping system, the water-cooling system, the air-pressure system, and the shielding against leakage radiation. The electron beam transport system brings the pulsed high-energy electron beam from the accelerating waveguide onto the target in the x-ray therapy mode and onto the scattering foil in the electron therapy mode.

The beam monitoring and beam collimation system forms an essential system in a medical linac ensuring that radiation dose may be delivered to the patient as prescribed, with a high numerical and spatial accuracy.

2.3.2 Linac Treatment Head

The linac head contains several components, which influence the production, shaping, localizing, and monitoring of the clinical photon and electron beams. Electrons, originating in the electron gun, are accelerated in the accelerating waveguide to the desired kinetic energy and then brought, in the form of a pencil beam, through the beam transport system into the linac treatment head, where the clinical photon and electron beams are produced. The important components found in a typical head of a modern linac include:

Several retractable x-ray targets;

- Flattening filters and electron scattering foils (also referred to as scattering filters);
- Primary and adjustable secondary collimators;

- Dual transmission ionization chambers;
- Field defining light and range finder;
- Optional retractable wedges or full dynamic wedges;
- Multileaf collimator (MLC).

Clinical photon beams are produced in medical linear accelerators with a target/flattening filter combination. The electron beam accelerated to a given kinetic energy in the accelerating waveguide is brought by the beam transport system onto an x-ray target in which a small fraction (of the order of 10%) of the electron pencil beam kinetic energy is transformed into bremsstrahlung x rays. The intensity of the x ray beam produced in the target is mainly forward peaked and a flattening filter is used to flatten the beam and make it useful for clinical applications. Each clinical photon beam produced by a given electron kinetic energy has its own specific target/flattening filter combination. Photon beam collimation in a typical modern medical linac is achieved with three collimation devices: the primary collimator, the secondary movable beam defining collimator, and the multileaf collimator (MLC). The primary collimator defines a maximum circular field which is further truncated with the adjustable rectangular collimator consisting of two upper and two lower independent jaws and producing rectangular or square fields with a maximum dimension of 40×40 cm^2 at the linac isocenter, 100 cm from the x-ray target.

The MLCs are a relatively new addition to modern linac dose delivery technology. In principle, the idea behind an MLC is simple. It allows production of irregularly shaped radiation fields with accuracy and efficiency and is based on an array of narrow collimator leaf pairs, each leaf controlled with its own miniature motor. The building of a reliable MLC system presents a substantial technological challenge and current models

incorporate up to 120 leaves (60 pairs) covering radiation fields up to 40×40 cm^2 and requiring 120 individually computer-controlled motors and control circuits.

Clinical electron beams are produced in a medical linac by retracting the target and flattering filter from the electron pencil beam and either scattering the electron pencil beam with a scattering foil or deflecting and scanning the pencil beam magnetically to cover the field size required for electron beam treatment. Special cones (applicators) are used to collimate the clinical electron beams.

Dose monitoring systems in medical linacs are based on transmission ionization chambers permanently imbedded in the linac clinical photon and electron beams. The chambers are used to monitor the beam output (patient dose) continuously during the patient treatment. In addition to dose monitoring the chambers are also used for monitoring the radial and transverse flatness of the radiation beam as well as its symmetry and energy. For patient safety, the linac dosimetry system usually consists of two separately sealed ionization chambers with completely independent biasing power supplies and readout electrometers. If the primary chamber fails during patient treatment, the secondary chamber will terminate the irradiation, usually after an additional dose of only a few percent above the prescribed dose has been delivered.

2.4 External Beam Radiation Therapy

External beam radiotherapy (EBT) also called external radiation therapy or teletherapy is a type of radiation therapy that makes use of a machine to direct high energy ionizing radiations to a tumor from outside the body. A beam of radiation is directed through the skin to the tumor and its immediate surroundings to destroy the tumor during external

beam radiotherapy. To achieve this, and minimize the radiation effect on the normal tissue, the treatments are fractionated for a number of weeks. Patients usually receive external beam radiation therapy in daily treatment sessions over the course of several weeks. The number of treatment sessions depends on many factors, including the total radiation dose that will be given. This allows enough radiation to be available in the body to kill the cancerous cells while giving the healthy cells time, each day, to recover.

External beam radiation is the most widely used type of radiation therapy, and it most often uses photon beams (either x-rays or gamma rays). A photon is the basic unit of light and other forms of electromagnetic radiation. It can be thought of as a bundle of energy. The amount of energy in a photon can vary. The photons in gamma rays have the highest energy, followed by the photons in x-rays. These radiation beams can be generated by 60Co machine, which produces gamma radiation or linear accelerator (also known as LINAC), producing high-energy x-rays beam. A LINAC uses electrical energy to form a stream of fast-moving subatomic particles. This creates high energy radiation that may be used to treat cancer.

By the help of high technique treatment planning software, the treatment team controls the size and shape of the beam, as well as how it is directed into the body, so as to treat the tumour effectively while sparing the surrounding normal tissue. EBT comes with many types depending on the beam energy, beam size and beam shape. These include: conventional external beam radiotherapy, stereotactic radiation therapy, three-dimensional conformal radiation therapy (3D-CRT), proton beam therapy, image guided radiation therapy (IGRT), particle therapy and neutron beam therapy.

2.4 Three Dimensional (3D) Conformal Radiation Therapy.

Three-dimensional (3D) conformal radiation therapy is a technique where the beams of radiation used in treatment are shaped to match the tumor. In some time past, radiation treatment matched the height and width of the tumor, meaning healthy tissues were exposed to the beams. Technological advancements in imaging have made it possible to locate and treat the tumor more precisely.

Conformal radiation therapy uses the targeting information to focus precisely on the tumor, while avoiding the healthy surrounding tissue. This is ideal for tumors that have irregular shapes or that lay close to healthy tissues and organs.

This exact targeting makes it possible to use higher levels of radiation in treating cancer cells, making it more effective in shrinking and killing tumors while limiting radiation exposure to surrounding healthy tissues.

Three-dimensional conformal therapy is, in diverse ways, similar to intensity-modulated radiation therapy (IMRT); both are used to target cancer cells while sparing healthy tissues. Using this radiation technology, we're first able to view a tumor in three dimensions with the help of image guidance. Based on these images, we then deliver radiation beams from several directions to the tumor.

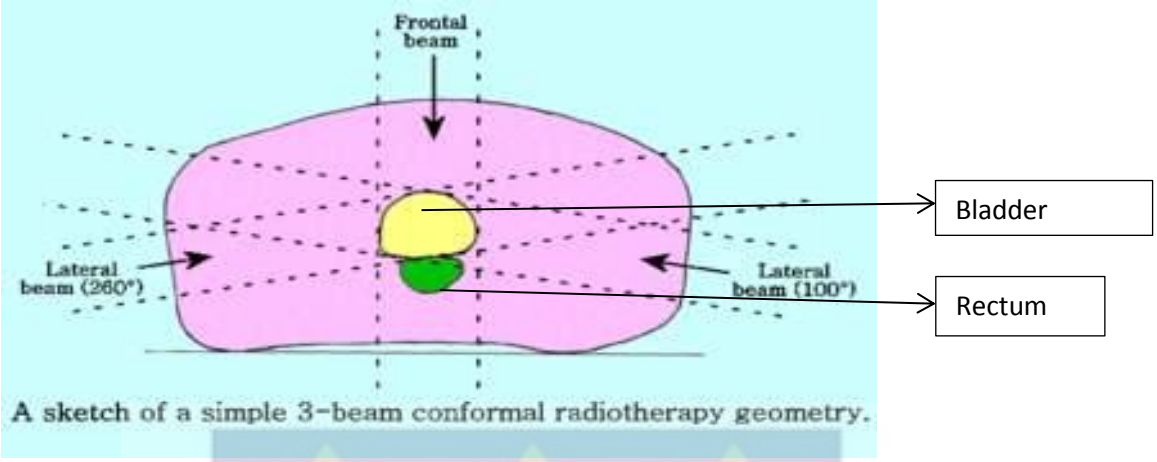

Fig 2.2 A Sketch of 3D conformal radiotherapy of a patient

2.4.1 Conventional External Beam Radiotherapy (CEBR)

CEBR is the type of external beam radiotherapy delivered through two-dimensional beams using linear accelerator machines (2DXRT) or cobalt 60 machines. It comprises of a single beam of radiation delivered to the patient from several directions: usually from front or back, and both sides of the patient.

Stereotactic radiation therapy is a specialized type of external beam radiation therapy that makes use of focused radiation beams targeting a well-defined tumor with the help of highly detailed image scans. Stereotactic radiation therapy comes in two types, namely;

- Stereotactic body radiation therapy (SBRT) and
- Stereotactic radiosurgery (SRS).

Stereotactic body radiation therapy (SBRT) and stereotactic radiosurgery (SRS) have been shown to be highly effective for the treatment of small and well-circumscribed brain metastases, with no regard of the primary site or histology. This suggests that small and well-circumscribed extracranial malignancies may be controlled with similar focal, high dose radiation therapy. However, it is difficult to administer such highly accurate

treatment to extracranial sites, because the lesions are movable even after the bony structures are fixed. These difficulties in targeting and localization of the lesions are overcome with the development of a novel treatment unit to achieve direct positioning of a moving target with a computed tomography (CT) scanner and immediate radiation therapy with a linear accelerator (linac). This type of radiotherapy is mainly used to treat very small cancers, including

- Cancer in the lung
- Cancer that started in the liver or cancer that has spread to the liver
- Cancers in the lymph nodes
- Spinal cord tumors

2.4.3 Stereotactic Body Radiation Therapy

Stereotactic Body Radiation Therapy (SBRT) is a treatment procedure which is similar to central nervous system (CNS) stereotactic radiosurgery. It is also referred to as stereotactic ablative radiotherapy (SABR). It deals with tumors outside of the CNS. A stereotactic radiation treatment for the body means that a specially designed coordinate-system is used for the exact localization of the tumors in the body in order to treat it with limited but highly precise treatment fields. SBRT involves the delivery of a single high dose radiation treatment or a few fractionated radiation treatments (usually up to 5 treatments). With SBRT, the tumour receives radiations from many different directions to attain accurate treatment. These radiations are high potent biological dose which improves the rate of cure for the tumour, in a manner previously not achievable by standard conventional radiation therapy.

It is a way of giving radiation to a tumour from many different directions to treat the target very accurately. Similarly, because this specialized form of radiation involves the use of multiple radiation beam angles, expert Radiation Oncologists specialized in this technique are able to safely deliver high doses of radiation, with very sharp dose gradient outside the tumor and into the surrounding normal tissue [18].

2.4.4 Intensity Modulated Radiation Therapy

Intensity modulated radiation therapy (IMRT) is a type of conformal radiation therapy. In CRT radiation beams are shaped to fit the area of the cancer. Intensity modulated radiation therapy (IMRT) uses hundreds of tiny radiation beam-shaping devices, known as collimators, to deliver a single dose of radiation. The collimators can be stationary or can move during treatment, thereby altering the intensity of the radiation beams during treatment sessions. This kind of dose modulation allows different areas of a tumor or nearby tissues to receive different doses of radiation.

Unlike other types of radiation therapy, IMRT is planned in reverse (called inverse treatment planning). For inverse treatment planning, the radiation oncologist chooses the radiation doses to different areas of the tumor and surrounding tissue, and then a high-powered computer program calculates the required number of beams and angles of the radiation treatment. In contrast, during traditional (forward) treatment planning, the radiation oncologist chooses the number and angles of the radiation beams in advance and computers calculate how much dose will be delivered from each of the planned beams.

The goal of IMRT is to increase the radiation dose to the areas that need it and reduce radiation exposure to normal tissues surrounding the tumor cells. The IMRT creates a U

shape (concave) around the edge of the tumour. Compared with 3D-CRT, IMRT can reduce the risk of some side effects, such as damage to the salivary glands (which can cause dry mouth, or xerostomia), when the head and neck are treated with radiation therapy. However, with IMRT, a larger volume of normal tissue overall is exposed to radiation. Comparison of IMRT with 3D-CRT as to whether it provides improved control of tumor growth and better survival is not yet known.

2.4.4 Image Guided Radiotherapy

In IGRT, the machines used are equipped with imaging technology that allows the physician to image the tumor before and during treatment for accurate radiation dose delivery. A number of these machines are linear accelerator (for x-ray or photon) or cyclotron/synchrotron (for proton) Image guided radiotherapy makes use of X-rays and scans similar to CT before and during radiotherapy treatment. The X-rays and scans show the size, shape and position of the cancer as well as the surrounding tissues and bones. Radiotherapy is made easier when the radiotherapy field covers the whole tumor with margins around it. During and between treatment, some areas of the body moves slightly. An example is the prostate gland which changes position according to the state of the bladder, whether full or not. This comes along with risk of the tumour being found outside the radiotherapy field. With some types of IGRT, the radiographers can take scans using the radiotherapy machine. This can be done before and/or during each treatment. Then they can make sure the cancer is within the radiotherapy field each time. Using specialized computer software, these images are then compared to the reference images taken during simulation. Any necessary adjustments are then made to the patient's position and/or radiation beams in order to more precisely target radiation at

the tumor and avoid healthy surrounding tissue. IGRT is used to treat tumors in areas of the body that are noted for movement, such as the lungs (affected by breathing), liver, and prostate gland, as well as tumors located close to critical organs and tissues. It is often used in conjunction with intensity-modulated radiation therapy (IMRT), proton beam therapy, stereotactic radiosurgery, or stereotactic body radiotherapy (SBRT), which are advanced modes of high-precision radiotherapy that utilize computer-controlled x-ray accelerators to deliver precise radiation doses to a malignant tumor or specific areas within the tumor. IGRT as importantly used for curative and palliative treatments, constitutes more than 50 % of all lung cancer treatment modalities.

2.5 Gamma Ray Beams and Gamma Ray Units

2.5.1 Basic properties of gamma rays

For use in external beam radiotherapy, γ-rays are obtained from specially designed and built sources that contain a suitable, artificially produced radioactive material.

The parent source material undergoes *f*>- decay, resulting in excited daughter nuclei that attain ground state through emission of γ - rays.

The important characteristics of radioisotopes in external beam radiotherapy are:

- High γ ray energy;
- High specific activity;
- Relatively long half-life;
- Large specific air kerma rate constant ΓAKR.

^{60}Co is the most widely used source, since it offers the most practical approach to external beam radiotherapy, considering the energy of emitted photons, half-life, specific activity and means of production.

2.5 Teletherapy machines

Treatment machines incorporating γ-ray sources for use in external beam radiotherapy are called teletherapy machines. They are most often mounted isocentrically, allowing the beam to rotate about the patient at a fixed SAD. Modern teletherapy machines have SADs of 80 cm or 100 cm. The main components of a teletherapy machine are: a radioactive source; source housing, including beam collimator and source movement mechanism; a gantry and stand in isocentric machines or a housing support assembly in stand-alone machines; a patient support assembly; and a machine console.

2.5.1 Teletherapy sources and encapsulation

The most widely used teletherapy source uses ^{60}Co radionuclide contained inside a cylindrical stainless steel capsule and sealed by welding. A double welded seal is used to prevent any leakage of the radioactive material.

- To facilitate interchange of sources from one teletherapy machine to another and from one isotope production facility to another, standard source capsules have been developed.
- The typical diameter of the cylindrical teletherapy source is between l and 2 cm; the height of the cylinder is about 2.5 cm. The smaller the source diameter, the smaller its physical penumbra and the more expensive the source is.

- Typical source activities are of the order of 5000 - 10.000 Ci (185 - 370 TBq) and provide a dose rate at 80 cm from the teletherapy source of the order of 100 - 200 cGy/min. Often the output of a teletherapy machine is stated in Rmm (roentgens per minute at 1 m) as a guide for the source strength.

2.5.2 Duration of source used and replacement

- Teletherapy sources are usually replaced within one half-life after they are installed; however, financial considerations often result in longer source usage.
- The Co-60 radionuclide in a teletherapy source decays with a half-life of 5.26 years into ^{60}Ni with the emission of electrons (P-particles) having a maximum energy of 320 keV and two y-rays with energies of 1.17 MeV and 1.33 MeV. The emitted y-rays constitute the therapy beam; the electrons are absorbed in the cobalt source or the source capsule, where they produce relatively low energy and essentially negligible bremsstrahlung x-rays and characteristic x-rays.

2.5.3 Physical properties of cobalt-60

Cobalt is a dense (mass density 8900 kg/m) silver white metal with a high melting point (1500 K); it is a non - radioactive ore rarely found in naturally occurring rock formation. The chemical symbol ^{60}Co, (atomic number 27, atomic weight 58.933 amu) is named for a globin. When cobalt-59 is bombarded with neutrons in a nuclear reactor, the resulting product is radioactive cobalt-60, with a half-life of 5.261 years and exposure rate constant of 1.31 $Rm^2h^1VCi^{-1}$

2.5.4 Teletherapy source housing

The housing for the teletherapy source is called the source head, and consists of a steel shell with lead for shielding purposes and a mechanism for bringing the source in front of the collimator opening to produce the clinical γ-ray beam. Currently two methods are in use for moving the teletherapy source from the beam off into the beam on position and back:

- A source on a sliding drawer and.
- A source on a rotating cylinder.

Both methods incorporate a safety feature in which the beam is terminated automatically in the event of a power failure or emergency.

- When the source is in the beam off position, a light source appears in the beam on position above the collimator opening, allowing an optical visualization of the radiation field, as defined by the machine collimators and any special shielding blocks.
- Some radiation will escape from the machine even when the source is in the off position. The head leakage is less than 1 mR/h (0.01 mSv/h) at 1 m from the source. International regulations also require that the average leakage of a teletherapy machine head be less than 2 mR/h (0.02 mSv/h) at 1 m from the source.

2.5.6 Dose delivery with teletherapy machines

The prescribed target dose is delivered with the help of two treatment timers: primary and secondary. The primary timer actually controls the treatment time; the secondary timer

serves as a backup timer in case of the primary timer's failure. The set treatment time must incorporate the shutter error, which accounts for the travel time of the source from the beam off position towards the beam on position at the start of irradiation and for the reverse travel at the end of irradiation.

2.6 Absolute and Relative Dosimetry

A radiation dosimeter is defined as any device that is capable of providing a reading M that is a measure of the dose D deposited in the dosimeter's sensitive volume V by ionizing radiation.

- A dosimeter that produces a signal from which the dose in its sensitive volume can be determined without requiring calibration in a known field of radiation is referred to as an absolute dosimeter;
- Dosimeters requiring calibration in a known radiation field are called relative dosimeters [53].

2.7 Central axis depth doses in water source to surface distance set -up

2.7.1 Percentage depth dose

Central axis dose distributions inside the patient or phantom are usually normalized to D_{max} = 100% at the depth of dose maximum z_{max} and then referred to as the PDD distributions. The PDD is thus defined as follows:

$$PDD\ (z, A, f, h\nu) = 100\ \frac{D}{Dr} = \frac{D^{\cdot}}{D^{\cdot}r} \qquad 2.1$$

Where D_Q, D'_Q are the dose and dose rate, respectively, at point Q at depth z on the central axis of the phantom and D_P, D_P are the dose and dose rate at point P at z_{max} on the central axis of the phantom. Point Q is an arbitrary point at depth z on the beam central axis; point P represents the specific dose reference point at z = z_{max} on the beam central axis. The PDD depends on four parameters: depth in a phantom z, field size *A*, SSD (often designated with *f)* and photon beam energy $h\nu$. The PDD ranges in value from 0 at z = 00 to 100 at z = z_{max}. The dose at point Q contains two components: primary and scatter.

- The primary component may be expressed as [29]:

$$PDD_{PRI} = 100\frac{D_Q^{PRI}}{D_P^{PRI}} = 100\left[\frac{f+Z_{max}}{f+Z}\right]^2 e^{-\mu_{eff}(z-z_{max})} \qquad 2.2$$

Where μ^{eff} is the effective linear attenuation coefficient for the primary beam in the phantom material (μ^{eff} for a ^{60}Co beam in water is 0.0657 cm).

- The scatter component reflects the relative contribution of the scattered radiation to the dose at point Q. The depth of dose maximum and the surface dose depend on the beam energy; the larger the beam energy, the larger the depth of dose maximum and the lower the surface dose. For constant z and $h\nu$ the PDD increases with increasing *A* because of increased scatter contribution to points on the central axis.
- For constant z, *A* and $h\nu$ the PDD increases with increasing/because of a decreasing effect of z on the inverse square factor, which governs the primary component of the photon beam.

- For constant z, A and hν the PDD beyond z_{max} increases with beam energy because of a decrease in beam attenuation (i.e. because of an increase in beam penetrating power).

The PDDs for radiotherapy beams are usually tabulated for square fields however, the majority of fields used in radiotherapy are rectangular or irregularly shaped. The concept of equivalent squares is used to determine the square field that will be equivalent to the given rectangular or irregular field.

2.8 Determination of absorbed dose under reference conditions

The absorbed dose to water at the reference depth z ref *in* water, in a photon beam of quality Q and in the absence of the chamber, is given by

$$D_{WQ} = M_Q \bullet N_{DWQ} \bullet k_{QQ}. \quad 2.3$$

Where M_Q is the reading of the dosimeter with the reference point of the chamber positioned at z_{ref} and corrected for the influence quantities temperature and pressure, electrometer calibration, polarity effect and ion recombination, N_{DWQ_0} is the calibration factor in terms of absorbed dose to water for the dosimeter at the reference quality Q_0, and $k_{Q,\ Q_0}$ is a chamber-specific factor which corrects for the difference between the reference beam quality Q_0 and the actual quality being used, Q [51].

2.8.1 Absorbed dose at z_{max}

However, clinical dosimetry calculations are often referenced to the depth of dose maximum z_{max} (or at some other depth). To determine the absorbed dose at the appropriate depth the user should, for a given beam, use the central axis percentage

depth-dose (PDD) data for SSD set-ups and tissue-phantom ratios (TPR) or tissue maximum ratios (TMR) for SAD set-ups [51].

2.8.2 Values for k_Q, Q_0

When the reference quality Q_0 is ^{60}Co, k_Q. Q_O is denoted by k_Q and N_{DWQo} is denoted by N_{DW}. These values have been adapted from the calculations of Andreo [52] and can be used at the reference depths. A sleeve of PMMA 0.5 mm thick has been used in the calculations for all the chambers which are not waterproof; for sleeve thicknesses up to 1 mm the change in k_Q is not greater than about 0.1%. Values of k_Q for non-tabulated qualities may be obtained by interpolation. It is emphasized that calculated k_Q values cannot distinguish chamber-to chamber variations within a given chamber type and their use necessarily involves larger uncertainties than directly measured values.

It should be noted that there is no value of Q that corresponds to ^{60}Co where all the k_Q values are equal to 1.000. While in principle there is a value of $TPR_{20.10}$ that would correspond to a pure ^{60}Co spectrum, the response of a particular chamber in an accelerator beam of the same $TPR_{20,10}$ depends on its energy response over the whole spectrum, and will not necessarily be the same as for ^{60}Co. In addition there is considerable disagreement in the literature as to what the $TPR_{20,10}$ of a ^{60}Co beam is (0.568 for the beam at the NPL; 0.572 in BJR 17, BJR 25 and at ARPANSA; 0.578 at NRC; 0.579, so that a single reference value cannot be used.

2.9 Radiation dose calculation

There are three main methods of dose calculation in use today. One class of algorithms is known as convolution, another as superposition, and the last as Monte Carlo analysis. Monte Carlo methods are the most accurate and also the most computationally intensive methods available. They are not used in clinical practice due to the enormous computational load they generate. Convolution and superposition methods are slightly less accurate, but can typically be computed in much less time than Monte Carlo methods.

2.10 Review of Works on the Motorized Wedge Output Factors and Other Wedge Factors.

Computing the dose at some reference point along the central beam axis and using off-axis factors and tissue maximum ratios or percentage depth doses to determine the radiation intensity at other points in the field is a method used to determine the radiation doses in wedged fields [2]. The dose at the central ray reference point of a wedged field was found by calculating the dose at the same point in an open field and multiplying it by the wedge factor (WF) in some time past when planning for treatment of patients. Wedge factors were measured at a field size and depth that was typical for treatment with the given wedge, and potential errors when treating with larger or smaller fields, or at different depths, were neglected. However, several investigators have demonstrated that the dependence of the WF on field size and depth is clinically important and that neglecting such dependence can lead to dosimetric errors greater than 5% [32]. As a result of this, later models of treatment-planning systems (TPSs) allowed input of wedge

factors for a series of square fields, and accepted separate depth dose or tissue maximum ratio data which took into consideration beam hardening by the wedge.

Turian et al, [2] made a report on the use of the EGS4/BEAM Monte Carlo technique in predicting the output factors for clinically relevant, irregularly shaped inserts as they intercept a linear accelerator's electron beams. The output factor for a particular combination—energy, cone, insert, and source-to-surface distance (SSD) — in accordance with AAPM TG-25 is defined as the product of cone correction factor and insert correction factor, evaluated at the depth of maximum dose. The goodness-of-fit between predicted and Monte Carlo–calculated ICF values was tested using the Kolmogorov–Smirnoff statistical test. The results showed that Monte Carlo–calculated ICFs matched the measured values within 2.0% for most of the shapes considered, except for few highly elongated fields, where deviations up to 4.0% were recorded. Predicted values based on analytical modeling agree with measured ICF values within 2% to 3% for all configurations. The predicted ICF values based on modeling of Monte Carlo–calculated values could be introduced in clinical use.

Popple et al, [3] reported that some modern treatment-planning systems (TPSs) provide for input of wedge factor (WF) tables covering the entire range of square and elongated fields available on the LINAC. Wedge factors computed from five to seven measurements comprised of square fields and a single, large rectangular field agreed with direct measurements throughout the entire range of achievable field dimensions within 0.6% at 6 MV and within 1% at 15 MV. Making the same set of measurements and using the equivalent square method to find WFs at other field sizes leads to errors up to 2%.

Measuring the WF for a 10 × 10 cm^2 field and applying the same value to all field sizes can lead to errors of up to 10% at both 6 MV and 15 MV.

A report on the dosimetric aspects of commissioning an Elekta Versa HD linear accelerator (linac) with high-dose-rate flattening filter-free (FFF) photon modes and electron modes was performed by Narayanasamy et al, [4]. In their research, acceptance and commissioning was performed on the Elekta Versa HD linac with five photon energies (6 MV, 10 MV, 18 MV, 6 MV FFF, and 10 MV FFF), four electron energies (6 MeV, 9 MeV, 12 MeV, and 15 MeV) and 160-leaf (5 mm wide) multileaf collimators (MLCs). Pinnacle Treatment Planning System (TPS) (Pinnacle ver. 9.8, Philips Healthcare, Eindhoven, Netherlands) was used to model the photon energies using the collapsed-cone convolution, and electron energies using the Hogstrom pencil-beam electron algorithms, using the data collected. The MLC transmission values were 0.5%, 0.6%, and 0.6% for 6 MV, 10 MV, and 18 MV photon beams, respectively. The electron PDDs, profiles, and cone factors agree well with the literature. The outcome of radiation treatment is directly related to the accuracy in the dose modeled in the treatment planning system, which is based on the commissioned data.

Hejazi et al, [50], investigated on wedge factor of the internal wedge of an Elekta linac for some wedge degrees for 6 MV photon beam using Monte Carlo (MC) methods. The wedge factors were calculated by the MC simulation of 60 and 30 and wedge with various dimensions of 4, 5, 10, 15 and 20 cm^2 and compared with relevant experimental measurements. The results indicated that the MC simulation can be regarded an accurate method for determining the wedge factor for all the wedge degrees. The MC method has

the potential for investigating the variation of medical linacs wedge factor with the field size.

2.11 The Oncentra MasterPlan Treatment Planning system.

Medical imaging is a tool mainly used to form a virtual patient for computer-aid design procedure. Geometry, radiology and dosimetric aspect of therapy are planned using treatment simulation and optimization [46]. In order for greater modulation to be attained by the intensity of radiation therapy, simulations are done by carefully selecting the required beam energy, beam arrangement, catheter positions and source dwell time [49]. The more optimization process is formal, the better the process could be referred to as forward planning or inverse planning [47].

Oncentra MasterPlan is a treatment planning system comprising of many individual treatment planning modules for external beam radiation therapy and brachytherapy. Oncentra is designed for DICOM integration, connectivity and flexibility. Oncentra MasterPlan TPS allows numerous sets of data points to be classified as applicator points [45]. For MasterPlan photon dose calculation, parameters such as energy deposition kernels, electron contamination kernels, fluence matrix, source size, head scatter, ionization chamber perturbation are required. In using WF value to determine the dose at isocentre (D_{iso}) and the maximum dose at d_{max}, (D_{zmax}), the following equations are used.

$$D_{iso} = mu \times D\,(z_{max}) \times ISF \times RDF \times WF \qquad 2.4$$

Therefore

$$WF = \frac{D_{iso}}{mu \times D\,(Z_{max}) \times ISF \times RDF} \qquad 2.5$$

Where mu is the monitor unit, ISF is the inverse square factor, RDF is the relative dose factor, and WF is the wedge factor, D (z_{max}) dose at depth of maximum dose.

CHAPTER THREE

3.0 MATERIALS AND METHODOLOGY

3.1 Introduction

This chapter describes the materials and the experimental methods used for this research. The research work was carried out using the Linear Accelerator Elekta Synergy platform, PMMA Solid Water Perspex slabs phantom and other equipment at the Sweden Ghana Medical Centre (SGMC).

3.2 Materials

The chapter outlines in details the experimental method and the materials employed in this research work carried out at Sweden Ghana Medical Centre, Accra. The materials used include:

- ELEKTA Platform Linear Accelerator with 6 MV and 15 MV Dual Energy.
- Solid Water Perspex Slabs Phantom (PMMA).
- Ionization chamber (PTW, farmer type 0.6 cm^3, PMMA/Al, 1 m)
- PTW UNIDOS Electrometer.
- Barometer.
- Thermometer.
- Oncentra master planner (4.3) version 4.3, software 4.3.0.410

3.2.1 Elekta Synergy Linear Accelerator unit

The radiotherapy unit at Sweden Ghana Medical Centre has one Elekta Synergy platform linear accelerator unit, a dosimetry room and an administrative set-up. The treatment

room containing the linear accelerator is used for external beam radiation treatment for all types of cancer treatment. The LINAC machine was installed at Sweden Ghana Medical Centre (SGMC) by Elekta a Swedish company in 2011.

This Elekta synergy platform linear accelerator at Sweden Ghana Medical Centre as seen in Fig 3.1 has both photon and electron energy. The photon energies produced are 6 MV, and 15 MV with electron energies of 6 MeV, 10 MeV and 15 MeV produced by the machine. The machine has a specialized multi-leaf collimator 2 x 40 leafs and 1 cm leaf width at isocentre. A 30 x 40 cm^2 wedge installed in the synergy platform permits a 40 cm maximum filed size at isocentre. It also has a motorized 60-degree wedge in place. In treatment delivery, the LINAC can be used to give three 3 dimensional radiotherapy, intensity modulated radiotherapy (IMRT), volumetric-modulated arc therapy (VMAT), stereotactic radiosurgery (SRS). The treatment couch used at Sweden Ghana Medical Centre is the precise and hexapod type. Fig 3.1 shows Pictorial view of the Synergy Platform Linear Accelerator unit at SGMC.

Figure 3.1 A Pictorial view of the Synergy Platform Linear Accelerator unit at SGMC.

3.2.2 PTW UNIDOS Electrometer

The type of electrometer at SGMC used for this study was a solid state electrometer called the PTW UNIDOS electrometer shown in Fig 3.2. It is an electrometer mainly used for daily routine dosimetry in radiation therapy. Ionization chambers and solid-state detectors can be connected. The chamber library makes it possible to store calibration data. This electrometer displaces measured values of dose and dose rate in Gy, R, Gy/min, R/min or Gy.m. The electrical values of charge and current are measured in coulombs (C) and ampere (A) respectively. The device has high contrast LC display which makes it easy for measured values to be read. Unidos electrometer automatically checks if there is high voltage between the electrodes of the ionization chamber so as to prevent damage to the ionization chamber.

The electrometer can be operated on both mains and battery power supply. Air density corrections are performed by keying-in air pressure and temperature or by means of a radioactive check device. The check device data are stored in a data babe. This electrometer has automatic noise suppression and automatic built-in system test. It is suitable for high precision dosimetry acceptance test of x-ray equipment using ionization chamber. It is very accurate, having long-term stability, excellent resolution and wide dynamic measuring ranges. It is suitable as a reference class dosimeter according to IEC 60731 for radiation therapy and as in-vivo dosimeter according to IEC 60601-2-9 for patient's dose measurement.

Figure 3.2 A pictorial view of the PTW UNIDOS E (webline Company, Germany) electrometer.

3.2.3 PTW Farmer Ionization Chamber (Type 30010)

The type of ionization chamber used at Sweden Ghana Medical Centre (SGMC) for this work was PTW Farmer Ionization Chambers. This type of ionization chamber PTW Farmer 30010 is intended for absolute and relative dosimetry photon and electron beams in radiotherapy. The ionization chamber used was calibrated against a source of known beam quality at the IAEA Secondary Standard Dosimetry Laboratory (SSDL). The calibration was done with a bias voltage of 400 V at the temperature of (23 °C), pressure of 100.5 kPa and humidity of 50%. The acrylic chamber wall ensures the ruggedness of the chamber. The chamber is designed for the use in solid state phantoms and therefore not waterproof. Measurements can be performed in air, water phantoms or solid phantoms. The PTW Farmer 30010 Ionization Chamber is an air ionization chamber vented through air. The chamber is designed for the use in solid state phantoms and therefore not waterproof. It is used for the measurement of dose rate, absorbed dose to water, air kerma or exposure for radiation therapy calibration measurements in air or solid phantom [17].

A thimble chamber (also known as compact chamber) consists of a central electrode and a cylindrical chamber wall with a spherical or conical end mounted on a cylindrical stem. A guard on central electrode potential leading up to the sensitive volume limits dark currents and stem effects. Thimble chambers are used for measuring high energy photon and electron radiation in air or in phantom material.

Features

- Vented sensitive volumes of 0.6 cm^3
- Suitable as therapy chambers for use in solid phantoms
- Flat energy response
- A variety of different versions is available

The 0.6 cm^3 PTW Farmer chambers are designed for absolute photon and electron dosimetry with therapy dosemeters. Three chamber types for measurements in air or in solid state phantom material are available:

- Type 30010 is the standard chamber. The wall material is graphite with a protective acrylic cover, and the electrode is made of Aluminium. The nominal photon energy range is from 30 kV to 50 MV.
- Type 30011 with graphite wall and graphite electrode is used for therapy dosimetry, where a completely graphite-built chamber is required. The nominal photon energy range is from 140 kV to 50 MV.
- Type 30012 is used for therapy dosimetry, where a chamber with graphite wall and Al electrode is required. The nominal photon energy ranges from 60 kV to 50 MV. The electron energy range of all chambers is from 6 MeV to 50 MeV. The chambers type 30011 and 30012 with their graphite caps are of delicate

construction and should be handled with extreme care. The guard rings of all chamber types are designed up to the measuring volume. An acrylic build-up cap for in-air measurement in ^{60}Co beams is included with each chamber as shown in Fig 3.3.

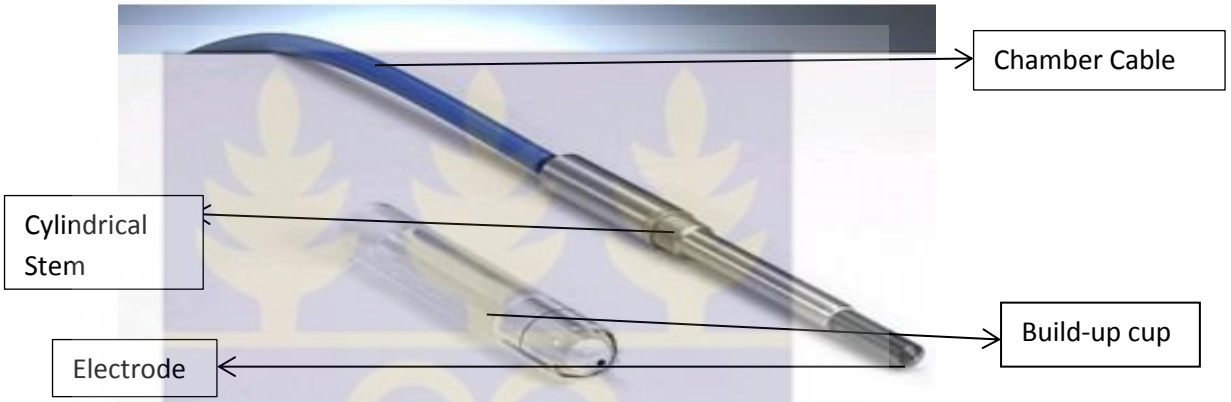

Figure 3.3 A pictorial view of the PTW 30010 Farmer Ionization Chamber.

3.3 Methodology

3.3.1 Experimental Setup

Figure 3.4 A Diagram of the Elekta Synergy linear accelerator, the PMMA Solid Water Slabs Phantom, Ionization chamber (PTW, farmer type 0.6 cm3, PMMA/Al, 1 m), thermometer Used for The Data Collection.

3.3.2 Absorbed Dose to Water Measurement

In this measurement, the PMMA Perspex solid slab phantom was placed on the lift table and the set up was left under the gantry. The distance from the source to the surface of the Perspex phantom (SSD) was adjusted by the help of the remote control to 100 cm. By the help of the lasers in the treatment room, the PTW farmer type ionization chamber was fixed into the Perspex phantom such that the sensitive part coincides with the cross point of the laser on the Perspex phantom's surface (that is; 100 cm SSD). All other

connections including the cable from the PTW farmer type ionization chamber to the PTW unidos electrometer and that of the thermometer were ensured to be rightly fixed. The central axis was defined. An MU of 100 was entered in the basic setting area. This permits the dose to be recorded for 100 MU at 1.5 and 2.5 cm d_{max} for both 6 and 15 MV. By selecting common setting, then choosing on measure option on the Omnipro-Accept software, the absorbed dose values were measured for 6 MV and 15 MV.

Motorized wedge output factors (MWOFs) of 6 and 15 MV photon beam energies were measured along the central axis using a Farmer-type ion chamber. Measurements were taken in a phantom composed of 30x30×30 cm^3 Solid Water Perspex slabs (Sweden Ghana Medical Centre, Accra) of varying thickness, with 15 cm of backscatter material to ensure full phantom scatter conditions. Other sheets of the solid water were added to take readings at the depth of maximum dose (d_{max}). The PMMA solid water slabs phantom was set to 100 cm SSD with the help of lasers aligned in the treatment room. The chamber was placed in the phantom such that the entrance window of the chamber was flushed with the surface with the central axis perpendicular to this at d_{max} of 1.5 cm and 2.5 cm for 6 MV and 15 MV respectively. Charges were collected for a fixed number of monitor units (100 MU) for each MDW angle using PTW Farmer 30010 ionization chamber and electrometer (PTW UNIDOS webline Company, Germany) for open field. Measurements were carried out with moving jaw Y1 for both collimator rotation 0° and 90°, so as to include setup errors. This was repeated for symmetric fields ranging from 5 to 30 cm using the same number of monitor units and set up.

3.3.3 Absolute dose measurement

Water phantom: PMMA Solid Water Perspex Slabs

Electrometer: PTW UNIDOS electrometer.

Chamber: PTW Farmer 30010

$N_{DjW} = 5.402\times10^{7}$ Gy/C $K_Q = 1.00$

Field size = 10x10 cm ^{2} SSD = 100 cm Z_{ref} = 1.5 cm d_{max}

Temp. = 23.0 °C Pressure = 100.5 kPa K_{Tp} = 1.0234

Measured dose:

3.3.4 Absolute dose measurement

Water phantom: PMMA Solid Water Perspex slabs.

Electrometer: PTW UNIDOS electrometer.

Chamber: PTW Farmer 30010

$N_{DjW} = 5.402\times10^{7}$ Gy/C $K_Q = 1.00$

Field size = 10x10 cm ^{2} SSD = 100 cm Z_{ref} = 2.5 cm d_{max}

Temp. = 23.0 °C Pressure = 100.5 kPa K_{Tp} = 1.0234

Measured dose:

The dose is then calculated from the equation 3.1 below,

$$D_{WQ} = M_Q \bullet N_{DWQ} \bullet k_{QQ}. \quad 3.1$$

3.3.5 Wedged Output Factor Determination

The ICRU® Report 24 [9] defines the WF of a given wedge with angle as

$$\text{WOF (a,b,w)} = \frac{\text{Dw(a,b,w)}}{\text{Do(a,b,o)}} \quad 3.2$$

Where D_w (a,b,w) is the dose at a specified point along the central ray in a field with dimensions a and b with the wedge in place, and D_o (a,b,o) is the dose to the same point in an open field of equal dimensions for the same time or number of MUs. If the wedge is manually inserted and the accelerator allows more than one direction of wedge insertion, the wedge factor also depends on the orientation of the wedge with respect to the collimator jaws, ot, so that Eq. (1) becomes

$$\text{WOF}(a,b,w) = \frac{Dw(a,b,w)}{Do(a,b,o)} \qquad 3.3$$

Wedge direction is defined as a vector pointing from the thick end to the thin end of the wedge. The wedge orientation can then be defined as the angle of the wedge direction relative to the collimator coordinate system. For a modern commercial LINAC, the wedge can be inserted in one of four possible orientations such that the direction is perpendicular to one of the collimator jaws. All four of the possible wedge orientations may not be available on a particular LINAC model. For symmetric collimator settings, orientations that are 180° apart should have the same WF. However, the radiation intensity profile for rectangular fields is not the same for orientations that are 90° apart. Therefore, it is not necessarily true that the WFs are the same for such wedge orientations. The dose in the presence of a wedge, D (a,b,w), is the sum of three components: dose from the primary beam, phantom scatter, and collimator scatter. Phantom scatter is the component of dose due to radiation scattered to the measurement point from within the phantom. Collimator scatter is the component of dose due to radiation scattered to the measurement point from within the treatment head and from the wedge itself. It has been demonstrated for both internally and externally mounted wedges

that phantom scatter is not significantly changed by the presence of a wedge and that the change in wedge factor with field size is determined primarily by changes in photon scatter from the wedge [43] and [10]. Photon scatter is nearly constant because the additional phantom scatter to the central axis from the thin side of the wedge is compensated by the deficit in scatter from the thick side of the wedge. Heukelom et al. [10] have observed that the magnitude of the wedge-induced change of the head scatter dose component is almost completely determined by the amount of irradiated wedge volume and, furthermore, that the WF is proportional to the irradiated wedge volume. If we assume that the wedge profile is linear and neglect beam divergence, then the irradiated wedge volume is proportional to the field area and is independent of wedge orientation with respect to the field. So the WF may be written as

$$WOF(a, b, w, ot) = WF(Aw) \quad 3.4$$

where A is the field area, A = ab, ot is the orientation of the wedge. This relationship between WF and field area was first suggested by Arthur et al [40], Popescu et al [39] also observed a linear dependence on field area for square fields. Furthermore, an investigation of in-air WFs for square fields demonstrated that for externally mounted wedges, the WF is proportional to field area [42].

To construct a full set of WFs requires measurements over the range of available field sizes F_x and F_y in appropriate increments. If the WF is different for wedge orientations that are 90° apart, a second set of measurements is required over the same range of field sizes. Assuming that the field size dependence of WFs is primarily due to scatter from the wedge and that the wedge scatter is proportional to the irradiated wedge volume, we expected WFs to be independent of orientation and to increase linearly with the area of

the radiation field. Because of this simple relationship, one needs to measure WFs at only a few selected field sizes, then one can determine the remaining values through linear interpolation; measurements are only necessary at one orientation. This approach significantly reduces the number of measurements otherwise required to determine a full set of field size-dependent WFs.

3.3.6 Data Analysis

A linear regression analysis was conducted to see if field size was a predictor of our measured MWOF. A one-way between subject's analysis of variance (ANOVA) was conducted to compare the effect of treatment planning system on the MWOF. To further evaluate the variance of output factor with field size by the Treatment Planning System the coefficient of variation (CV) was calculated. The standard formulation of the CV is the ratio of the standard deviation to the mean multiplied by 100. All these statistical analyses were carried out using Microsoft Excel version 14.0.4760.1000 (2010).

CHAPTER FOUR

4.0 RESULTS

4.1 Field Size Dependence

The Wedge output factor (MWOF) for 6 MV and 15 MV photon beams for field sizes of 5×5 cm^2, 10×10 cm^2, 15×15 cm^2, 20×20 cm^2, 25×25 cm^2, 30×30 cm^2 measured are given in detail from table 4.1 and 4.2 respectively. The measurement precision varies from 0.1% to 0.5%. When the MWOF as a function of field size was analyzed using simple linear regression analysis, the coefficients varied from 0.971 to 0.988 for 6 MV and 0.141 to 0.892 for 15 MV. The MWOF values for 6 MV and 15 MV photon energy at 100 cm SSD for the various square field sizes are presented in Tables 4.1 and 4.2.

Table 4.1 A Table Showing Field Sizes, Wedge Angles with Their Corresponding MWOF for 6 MV.

	FIELD SIZES					
WEDGE ANGLES	5×5	10×10	15×15	20×20	25×25	30×30
15	0.712249	0.719625	0.722492	0.725892	0.727363	0.728143
30	0.53628	0.543922	0.557632	0.553401	0.556398	0.557806
45	0.399469	0.407258	0.41286	0.419467	0.423391	0.425537
60	0.338122	0.290223	0.289168	0.296928	0.301633	0.304413

Table 4.2 A Table Showing Field Sizes, Wedge Angles with Their Corresponding MWOF for 15 MV.

	FIELD SIZES					
WEDGE ANGLES	5×5	10×10	15×15	20×20	25×25	30×30
15	0.712249	0.719625	0.722492	0.725892	0.727363	0.728143
30	0.53628	0.543922	0.557632	0.553401	0.556398	0.557806
45	0.399469	0.407258	0.41286	0.419467	0.423391	0.425537
60	0.338122	0.290223	0.289168	0.296928	0.301633	0.304413

MWOF values of 6 MV were lower than 15 MV for all field sizes as seen in Tables 4.1 and 4.2. The absorbed dose for 6 MV, and 15 MV photon beams for various field sizes were measured with the slabs of plastic phantom (PMMA) at 1.5 cm and 2.5 cm d_{max} respectively. It was observed from Tables 4.3 and 4.4 that a maximum deviation of MWOF values ±0.55% and ±4.11% were observed in various field sizes ranging from 5×5 cm^2 to 30×30 cm^2 for 6 MV and 15 MV respectively from the PMMA plastic slabs phantom measured values. The MWOF was higher for 15 wedges than the rest of the wedges and lowest for 60° wedges from 5×5 cm^2 to 30×30 cm^2. There is a linear positive dependence of MWOF with field size (FS). The wedge angle also had an effect on dependence of MWOF on FS, as the field size increased the wedge angle decreased. The MWOF increase as the field size increases and decreases with wedge angle for 6 MV but increases from 5×5 cm^2 to 20×20 cm^2 for 45 wedge and increases again from 20×20 cm^2 to 30×30 cm^2 for 15 MV.

Table 4.3 Shows Field Sizes, Wedge Angles, Wedge Output Factors for Both Measured and TPS Data (MWOF Cal.), Mean, Difference, %Difference, Standard Deviation, %Standard Deviation and Coefficient of Variation for 6 MV Photon Energy.

FS	WA	MWOF Cal.	MWOF Mea.	Mean	Diff.	% Diff.	STD	% STD	COV
	15	0.7053	0.7071	0.7062	0.0019	0.273	0.0014	0.1362	0.1928
5*5	**30**	0.5263	0.5255	0.5259	-0.0008	-0.158	0.0006	0.0587	0.1117
	45	0.3895	0.3878	0.3887	-0.0016	-0.423	0.0012	0.1162	0.2990
	60	0.2632	0.2629	0.2630	-0.0003	-0.108	0.0002	0.0201	0.0762
	15	0.7172	0.7094	0.7133	-0.0078	-1.096	0.0055	0.5525	0.7746
10*10	**30**	0.5253	0.5291	0.5272	0.0038	0.721	0.0027	0.2689	0.5101
	45	0.3939	0.3925	0.3932	-0.0015	-0.369	0.0010	0.1025	0.2606
	60	0.2727	0.2687	0.2707	-0.0041	-1.508	0.0029	0.2886	1.0661
	15	0.7157	0.7114	0.7136	-0.0043	-0.598	0.0030	0.3019	0.4230
15*15	**30**	0.5343	0.5330	0.5337	-0.0013	-0.247	0.0009	0.0932	0.1746
	45	0.4020	0.3975	0.3997	-0.0045	-1.119	0.0032	0.3164	0.7915
	60	0.2745	0.2748	0.2747	0.0003	0.121	0.0002	0.0235	0.0856
	15	0.7164	0.7143	0.7153	-0.0021	-0.293	0.0015	0.1482	0.2071
20*20	**30**	0.5385	0.5372	0.5379	-0.0012	-0.228	0.0009	0.0867	0.1612
	45	0.3990	0.4003	0.3997	0.0013	0.314	0.0009	0.0887	0.2220
	60	0.2789	0.2814	0.2801	0.0025	0.896	0.0018	0.1774	0.6333
	15	0.7177	0.7159	0.7168	-0.0019	-0.257	0.0013	0.1305	0.1820
25*25	**30**	0.5359	0.5397	0.5378	0.0038	0.705	0.0027	0.2679	0.4982
	45	0.4067	0.4061	0.4064	-0.0006	-0.156	0.0005	0.0448	0.1101
	60	0.2823	0.2850	0.2837	0.0028	0.969	0.0019	0.1943	0.6848
	15	0.7177	0.7163	0.7167	-0.0014	-0.201	0.0010	0.1021	0.1424
30*30	**30**	0.5359	0.5408	0.5383	0.0049	0.902	0.0034	0.3435	0.6380
	45	0.41145	0.4076	0.4096	-0.0039	-0.951	0.0028	0.2754	0.6725
	60	0.28709	0.2870	0.2870	-0.00001	-0.032	0.00001	0.0065	0.0226

Table 4.4 Table 4.4 Shows Field Sizes, Wedge Angles, Measured and Calculated Motorised Wedge Output Factors, Mean, Difference, %Difference, Standard Deviation, %Standard Deviation and Coefficient of Variation for 15 MV Photon Energy.

FS	WA	MWOF Cal.	MWOF Mea.	Diff	% Diff	Mean	STD	% STD	COV
	15	0.7174	0.7123	0.0051	0.719	0.7148	0.0036	0.364	0.509
5*5	**30**	0.5544	0.5363	0.0181	3.313	0.5453	0.0128	1.278	2.343
	45	0.4130	0.3995	0.0136	3.341	0.4063	0.0096	0.960	2.363
	60	0.3424	0.3381	0.0043	1.255	0.3403	0.0030	0.302	0.887
	15	0.7231	0.7196	0.0035	0.478	0.7214	0.0024	0.244	0.338
10*10	**30**	0.5539	0.5439	0.0099	1.811	0.5489	0.0070	0.703	1.280
	45	0.4103	0.4073	0.0030	0.736	0.4088	0.0021	0.213	0.521
	60	0.3484	0.2902	0.0582	18.223	0.3193	0.0411	4.115	12.886
	15	0.7327	0.7225	0.0102	1.399	0.7276	0.0072	0.720	0.990
15*15	**30**	0.5545	0.5576	-0.0032	-0.571	0.5560	0.0023	0.225	0.404
	45	0.4257	0.4129	0.0129	3.072	0.4193	0.0091	0.911	2.173
	60	0.2970	0.2892	0.0079	2.682	0.2931	0.0056	0.556	1.897
	15	0.7304	0.7259	0.0045	0.618	0.7281	0.0032	0.318	0.437
20*20	**30**	0.5490	0.5534	-0.0044	-0.795	0.5512	0.0031	0.310	0.562
	45	0.4216	0.4195	0.0021	0.500	0.4205	0.0015	0.149	0.353
	60	0.3039	0.2969	0.0070	2.328	0.3004	0.0050	0.495	1.646
	15	0.7282	0.7274	0.0008	0.109	0.7278	0.0006	0.056	0.077
25*25	**30**	0.5631	0.5564	0.0067	1.199	0.5598	0.0047	0.474	0.847
	45	0.4272	0.4234	0.0038	0.892	0.4253	0.0027	0.268	0.631
	60	0.3010	0.3016	-0.0007	-0.220	0.3013	0.0005	0.047	0.156
	15	0.7282	0.7281	0.00001	0.002	0.7282	0.0001	0.001	0.001
30*30	**30**	0.5631	0.5578	0.005	0.946	0.5605	0.0038	0.375	0.669
	45	0.4272	0.4255	0.002	0.387	0.4264	0.0012	0.117	0.273
	60	0.3010	0.3044	-0.003	-1.137	0.3027	0.0024	0.243	0.804
STD		0.1603	0.1576			0.1589			1.377

The MWOF values ranged from 0.29 to 0.71 for 6 MV and 0.30 to 0.71 for 15 MV. The MWOF values of 15 MV were higher than 6 MV thereby the mean of 15 MV being higher than the mean of 6 MV. A significant variation in MWOF values was observed in

6 MV compared to 15 MV and a variation of only 0.60% was observed over the entire range of 5 × 5 cm^2 to 30 × 30 cm^2 field sizes for 6 MV compared to 1.39% for 15 MV.

From fig 4.2 the MWOF also increases from 5×5 cm^2 to 10×10 cm^2 and then from 15×15 cm^2 to 30×30 cm^2 for 15° wedge for 15 MV. The same trend is observed in the 15° wedge for 6 MV in Fig 4.1.

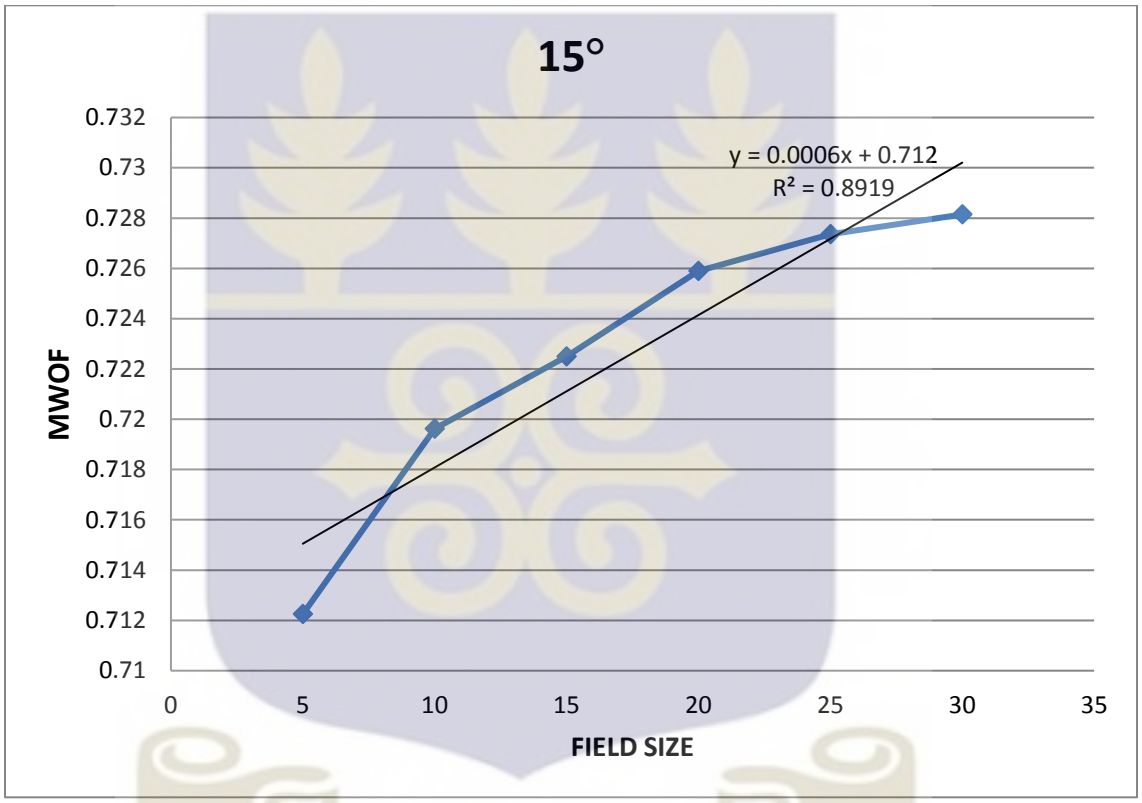

Figure 4.1 A Graph of Motorized Wedge Output Factor and Field Size for 15°, 15 MV.

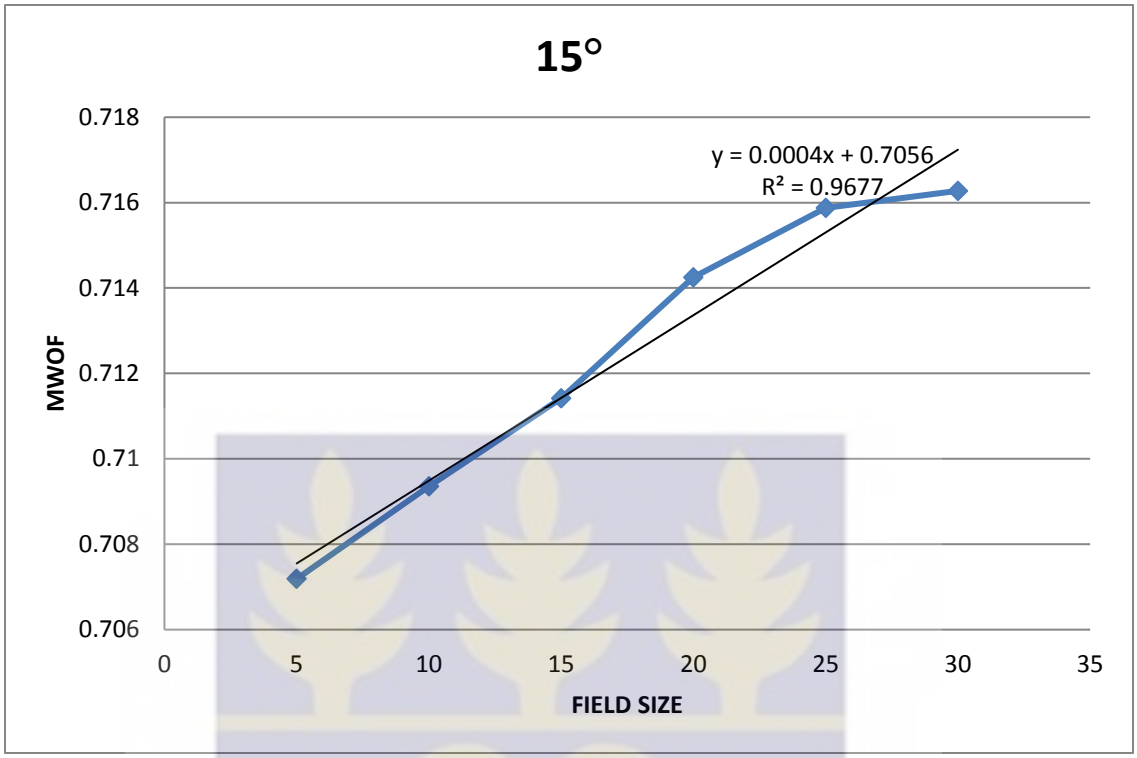

Figure 4.2 A Graph of Motorized Wedge Output Factor and Field Size for 15°, 6 MV.

4.2 Wedge Angle Dependence

The WA also had an effect on dependence of MWOF on FS. The highest change in MWOF with field size is for the 60° wedge. For example, there is a 1.8% increase in wedge factor between 5 ×5 cm^2 to 20 ×20 cm^2 for 60° wedge as compared to 1.0% for 15° wedge for 6 MV as seen in Tables 4.5 and 4.6.

Table 4.5 A Table of Values showing, Difference, Percentage difference, Mean, Standard Deviation, % Standard Deviation and COV for 6 MV, 60° Wedge.

60° WEDGE								
FIELD SIZE	**Cal. WOF**	**Mea. WOF**	**Difference**	**% Difference**	**Mean**	**Stdev**	**% Stdev**	**COV**
5×5	0.263158	0.262874	0.000284	0.107768	0.263017	0.000201	0.020053	0.076244
10×10	0.272727	0.268646	0.004081	1.496463	0.270687	0.002886	0.288589	1.066136
15×15	0.27451	0.274842	-0.000332	-0.121114	0.274677	0.000235	0.023509	0.085589
20×20	0.278846	0.281355	-0.002509	-0.899669	0.280101	0.001774	0.177391	0.633313
25×25	0.28228	0.285027	-0.002747	-0.973163	0.283654	0.001942	0.194246	0.684798
30×30	0.287088	0.286996	0.00001	0.031969	0.287042	0.00001	0.00649	0.022609
STD	0.008333	0.009555		0.894631			0.117811	
%STD	0.833307	0.955462		89.46313				

Table 4.6 A Table of Values showing, Difference, Percentage difference, Mean, Standard Deviation, % Standard Deviation and COV for 15 MV, 60° Wedge

MW 60 degree								
FIELD SIZE	**Cal. WOF**	**Mea. WOF**	**Difference**	**% Difference**	**Mean**	**Stdev**	**% Stdev**	**COV**
5×5	0.342391	0.338122	0.004269	1.246953	0.340257	0.003019	0.301896	0.887261
10×10	0.348412	0.290223	0.058189	16.70111	0.319317	0.041146	4.114555	12.88548
15×15	0.29703	0.289168	0.007861	2.646698	0.293099	0.005559	0.555891	1.896597
20×20	0.303922	0.296928	0.006993	2.300973	0.300425	0.004945	0.494491	1.64597
25×25	0.300971	0.301633	-0.00066	-0.22007	0.301302	0.000468	0.046836	0.155445
30×30	0.300971	0.304413	-0.00344	-1.14364	0.302692	0.002434	0.243388	0.804079
STD	0.023254	0.018043			0.017362			

As would be expected, the wedge factors increase with energy. Wedge factors measured for each available wedge and for different field sizes at depth of maximum dose (d_{max}) present a maximum variation with field size of 1.06% and 18% for both 6 and 15 MV units respectively from FS = 5 cm to 20 cm with the 60° wedge.

4.3 Comparison of MWOF to TPS Data.

The measured MWOF compared very well with the calculated MWOF (TPS data) from Tables 4.3 and 4.4. However, comparing the results with that from the Treatment Planning System data, an excellent agreement for 6 MV MWOF with the percentage differences ranging from 0.03% to 1.51%, with a mean of 0.11% was established. However, for 15 MV, the MWOF showed good agreement, ranging from 0.001% to 18.22%, with a mean of 1.72%. This is comparable to a study conducted by Popple et al, [3] where the MWOF was found to be within 1% and 10%. As expected, there was good agreement between the higher wedge angles for the 15 MV and the TPS data. The mean MWOF, standard deviation, and coefficient of variation (COV) are illustrated in Tables 4.1 and 4.2. The COV for a single variable describes the dispersion of the variable in a way that does not depend on the variable's measurement unit. The higher the COV, the greater the dispersion in the variable. In this study, the dispersion of the MWOF for the different field sizes is shown in Tables 4.1 to 4.2 with the MWOF COV ranging from 0.02% to 1.06% for the 6 MV. For 15 MV the COV ranged from 0.01% to 12.89%. This observed variation between the computed results from the measured data and the TPS data is within experimental errors. Analysis of variance (ANOVA) was used to evaluate the differences in the data between the computed MWOF and that of the TPS data. For 6 MV photon energy MWOF (Table 3) there was no significant difference between the computed MWOF and the TPS ($F(2, 25) = 0.00027$, p-value = 0.989). Also, there was no significant difference for reported MWOF for 15 MV ($F(3, 26) = 0.0234$, p-value = 0.879). The data in Tables 4.1 - 4.8 are further confirmation that the MWOF can be represented by a single database.

Table 4.7 A table of Values showing, Difference, Percentage difference, Mean, Standard Deviation, % Standard Deviation and COV for 6 MV, 15° Wedge.

15° WEDGE								
FS	**Cal. MWOF**	**Mea. MWOF**	**Difference**	**% Difference**	**Mean**	**Stdev**	**% Stdev**	**COV**
5×5	0.705263	0.707189	-0.001926	-0.273021	0.706226	0.00136	0.13616	0.192792
10×10	0.717172	0.709358	0.007814	1.089496	0.713265	0.00553	0.55250	0.77461
15×15	0.715686	0.711417	0.004269	0.596468	0.713552	0.00302	0.30185	0.423028
20×20	0.716346	0.714251	0.002095	0.292468	0.715299	0.00148	0.14815	0.207109
25×25	0.71772	0.715874	0.001845	0.257112	0.716797	0.00131	0.13049	0.18204
30×30	0.71772	0.716276	0.001444	0.201209	0.716998	0.00102	0.10212	0.14242

Table 4.8 A table of Values showing, Difference, Percentage difference, Mean, Standard Deviation, % Standard Deviation and COV for 6 MV, 30° Wedge.

30° WEDGE								
FS	**Cal. MWOF**	**Mea. MWOF**	**Difference**	**% Difference**	**Mean**	**Stdev**	**%Stdev**	**COV**
5×5	0.526316	0.525485	0.000831	0.157791	0.525901	0.00059	0.05872	0.11166
10×10	0.525253	0.529055	-0.003803	-0.724007	0.527154	0.00269	0.26890	0.51010
15×15	0.534314	0.532996	0.001318	0.246622	0.533655	0.00093	0.09318	0.17460
20×20	0.538462	0.537235	0.001227	0.227770	0.537848	0.00087	0.08672	0.16124
25×25	0.535897	0.539686	-0.003789	-0.707028	0.537792	0.00268	0.26792	0.49818
30×30	0.535897	0.540755	-0.004857	-0.906399	0.538326	0.00344	0.34347	0.63803

4.4 Discussion

4.4.1 MWOF — Dependence on Field Size

There was a linear dependence of MWOF with some field sizes and this agrees with what has been reported by Popple et al, 2005. The dependence of MWOF with field size is more pronounced with thicker wedge. As seen in the Fig 4.3, the MWOF increases linearly with increase in field size up to 20×20 cm^2 field size. There is further increase from the 20×20 cm^2 to 30×30 cm^2. The further increase is not linear as compared to field sizes ranging from 5×5 cm^2 to 20×20 cm^2. Fig.4.4 is the plot of MWOF against field size. It can be seen from the figure that for 45° wedge, the linearity is from 5×5 cm^2 to 15×15 cm^2 and continues from 15×15 cm^2 to 30×30 cm^2.

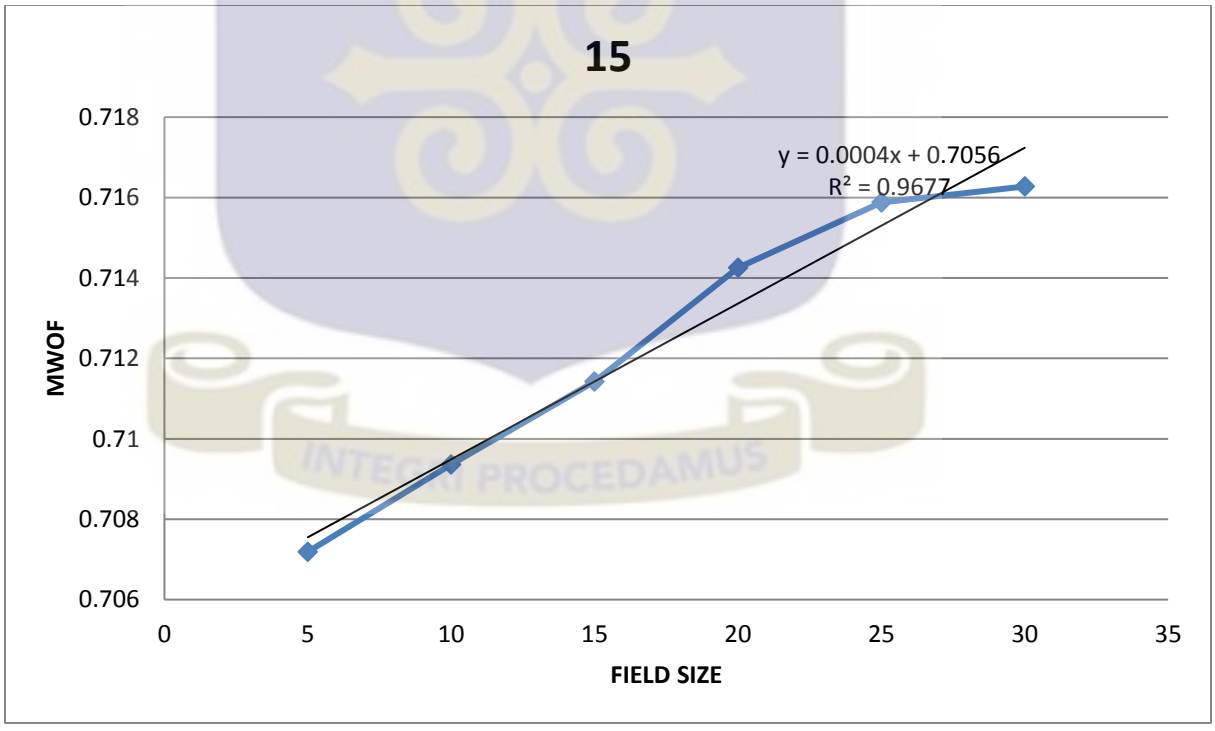

Figure 4.3 A Graph of Motorized Wedge Output Factor and Field Size for 15° Wedge 6 MV.

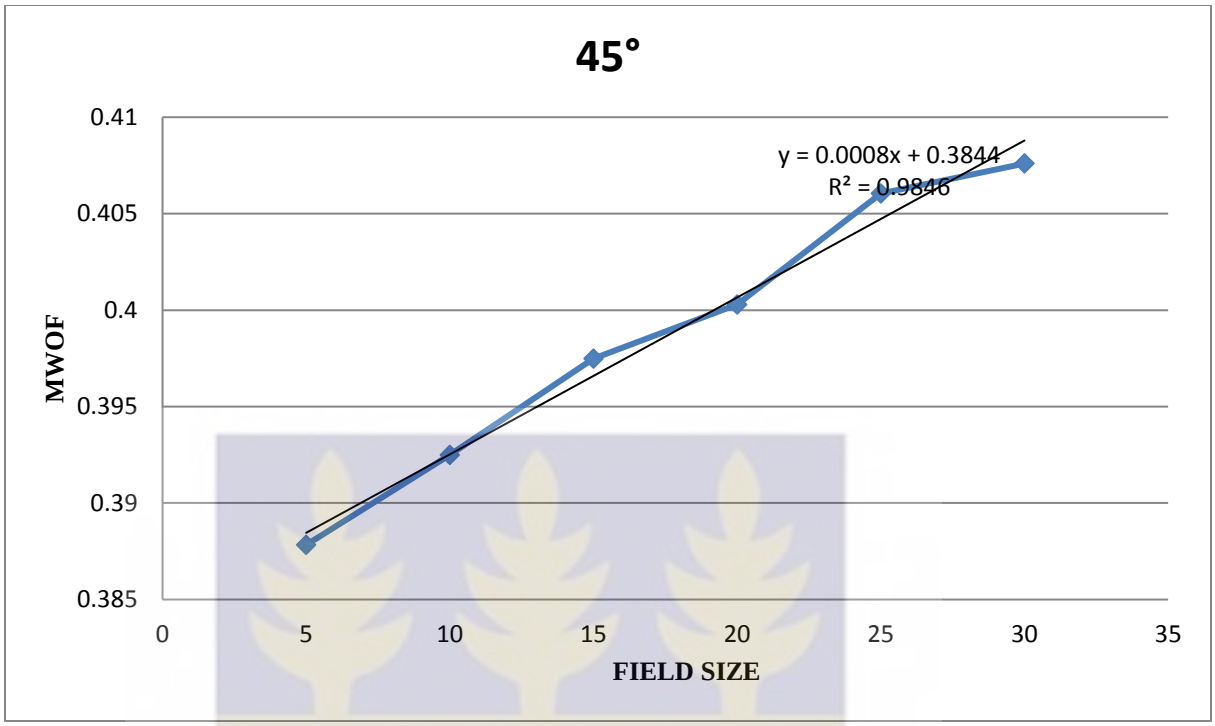

Figure 4.4 A Graph of Motorized Wedge Output Factor and Field Size for 45° Wedge 6 MV.

Linearity would exist if the WF were proportional to scatter from the wedge, wedge scatter was proportional to field size, and photon scatter from the wedge originated as if from an isotropic point source located on the central axis. However, the angular distribution of scatter will introduce additional dependence on both field size and shape, the scatter is not linearly related to field size, and the scatter originates from within the wedge volume rather than from a point. In addition, the relationship between WF and irradiated wedge volume observed by Heukelom et al, [38] was subsequently demonstrated to be not as strong as originally suggested. Nevertheless, the relationship is piecewise linear, suggesting that measurements at a few field sizes can be used to estimate the WF at an arbitrary field size.

4.4.2 Comparison of MWOF with the TPS Data

The MWOF for 6 MV and 15 MV photon energy of Elekta Synergy have been reported. As evident in Tables 4.3 and 4.4, there is a good agreement between the MWOF computed from dose measurement and the TPS data for 6 MV and 15 MV ($F(2, 25) = 0.00027$, p-value = 0.989). Also, there was statistically significant difference for reported MWOF for 15 MV ($F(3, 26) = 0.0234$, p-value = 0.879). Comparing the different values of MWOF for the measured doses and the TPS data, Pearson coefficient indicates a very good concordance ($r = 0.9998$ and 0.9972) for 6 MV and 15 MV respectively (depicting a strong positive correlation between MWOF of the measured values and the TPS data. The computed MWOF and that of the TPS data showed deviations of less than 1% for 6 MV photon energy across all field sizes. For 15 MV the deviation was up to 4% compared to the work done by Popple et al, [3] where Wedge factors computed from five to seven measurements comprised of square fields and a single, large rectangular field agreed with direct measurements throughout the entire range of achievable field dimensions within 0.6% at 6 MV and within 1% at 15 MV. %. Also, comparing our MWOF results (for 15 MV) with the Treatment Planning System data in Tables 4.4, MWOF shows good agreement. The agreement ranges from 0.001% to 18.22%, with a mean of 1.72% with Ahmad et al, [38] observed a non-significant variation of Enhanced dynamic wedge factor with depth, they found up to 8.9% variation in 60° physical wedge with depth for a 6 MV photon. This lack of depth dependence for dynamic wedge can be explained by the absence of beam hardening. Comparing the MWOF in Tables 4.1 and 4.2 for both 6 MV and 15 MV photon energies, it is observed that the MWOF of the measured data is lower than that of the TPS data. As the MWOF of the TPS data for 6

MV and 15 MV are compared, there is an increase in the MWOF as the photon energy increases and this is in agreement to a study by Njeh et al, [32] on enhanced dynamic wedge output factors. They observed an increase in wedge output factors as the photon energy increases.

CHAPTER FIVE

5.0 CONCLUSION AND RECOMMENDATION

5.1 Conclusion

In radiotherapy practice, using more than one radiation beam in external photon beam radiotherapy helps achieve a uniform dose distribution inside the target volume with healthy tissues surrounding the target receiving as low as possible a dose. High energy beam makes use of wedged fields for isodose distribution modification by compensating dose inhomogeneity in radiotherapy treatments.

MWOFs were computed from measured absorbed dose values for wedge fields and open fields for 6 MV and 15 MV respectively.

There was a linear positive dependence of MWOF with field size (FS). The wedge angle also had an effect on dependence of MWOF on FS, as the field size increased the wedge angle decreased. Wedge scatter was proportional to field size, and photon scatter from the wedge originated from an isotropic point source located on the central axis. However, the angular distribution of scatter introduced additional dependence on both field size and shape, making the scatter not to linearly relate to field size when the scatter originates from within the wedge volume rather than from a point.

The MWOF from the measured data compared very well with the Treatment Planning System. An agreement was found for 6 MV MWOF with the percentage differences ranging from 0.03% to 1.51%, with a mean of 0.11%. MWOF results for 15 MV also showed good agreement. The p-values had for predicting the differences in data for the measured MWOF and that of the TPS showed statistically significant difference. The

ANOVA values were a confirmation that the MWOF could be represented by a single database.

Pearson coefficient (r = 0.9998 and 0.9972) for 6 MV and 15 MV respectively showed a strong positive correlation between MWOF for the measured values and the TPS data.

The measured MWOF and that of the TPS data, showed deviations of less than 1% across all field size for 6 MV and 4% for 15 MV. The MWOFs were determined for 6 MV and 5 MV Elekta Synergy and the results from the measured data compared to the TPS data.

5.2 Recommendations

The following are recommendations are suggested to the various stake holders in the administration of dose to patient and also patient's protection from ionizing radiation.

5.2.1 Medical professionals

Based on the agreement between the measured and the calculated MWOFs, the measured MWOF data at SGMC and the calculation method can be used for double check during beam commission so as to check on the performance of the measuring system.

Also, it is recommended that, calculated Motorized Wedge Output Factor can confidently be used in calculating monitor units especially when applying both large and small field sizes to treat shallow tumors for high megavoltage x-ray beam.

5.2.2 Sweden Ghana Medical Centre

Since there was slight deviation when the measured data was compared with that obtained on the treatment planning system during commission, it is recommended that comparison of the measured MWOF with that obtained during commission should be included in the annual quality assurance (QAs) of the machine.

5.2.3 Regulators

It is recommended that the Regulatory Authority (RA), inspects compliance on radiation and dosimetric equipment so as to ensure patient's safety and avoidance of overexposure or underexposure during the administration of radiation treatment.

5.2.4 Further research work

The study could be further extended by considering various electron energies, addition of asymmetric fields, measuring at different depth in a phantom.

REFERENCES

[1] Verhaegen F, Mubata C, Pettingell J, Bidmead AM. Monte Carlo calculation of output factors for circular, rectangular and square fields of electron accelerators (6-20 MeV). Med Phys. 2001; 28:938–949.

[2] Julius V. Turian, Brett D. Smith, Damian A. Bernard, Katherine L. Griem, and James C. Chu. Monte Carlo calculations of output factors for clinically shaped electron fields: 2004.

[3] Richard A. Popple, Ivan A. Brezovich, Jun Duan, Sui Shen, Prem N. Pareek, and Sung-Joon Ye. Determination of field size-dependent wedge factors from a few selected measurements: 2004.

[4] Ganesh Narayanasamy, Daniel Saenz, Wilbert Cruz, Chul S. Ha, Niko Papanikolaou, and Sotirios Stathakis. Commissioning an Elekta Versa HD linear accelerator: 2015.

[5] Klein EE. Treatment planning for enhanced dynamic wedge with the CMS focus/Modulex treatment planning system. Med Dosim. 1997; 22(3):213–14.

[6] Leavitt DD. Dynamic beam shaping. Med Dosim. 1990; 15(2):47–50.

[7] Shao H, Wu X, Luo C, Crooks A, Bernstein A, Markoe A. The accuracy of dynamic wedge dose computation in the ADAC Pinnacle RTP system. J Appl Clin Med Phys. 2004; 5(4):46–54.

[8] Alaei P and Higgins PD. Performance evaluation and quality assurance of Varian enhanced dynamic wedges. J Appl Clin Med Phys. 2006; 7(1):14–20.

[9] ICRU (International Commission on Radiation Units and Measurements). Determination of absorbed dose in patients irradiated by beams of x or gamma rays in radiotherapy procedures. Report 24, 2004.

[10] Kapanen M, Sipila P, Bly R, Jarvinen H, Tenhunen M. Accuracy of central axis dose calculations for photon external radiotherapy beams in Finland: the quality of local beam data and the use of averaged data. Radiother Oncol. 2008; 86(2):264–71.

[11] Watts RJ. Comparative measurements on a series of accelerators by the same vendor. Med Phys. 1999; 26(12):2581–85.

[12] C.P Walkeral, N.D Richmonda 1,Optimal clinical implementation of the Siemens Virtual Wedge ,Top of Form Bottom of Form Received 3 April 2002; accepted 3 March 2003 .

[13] Petti Paula L, Siddon Robert L. Effective wedge angles with a universal wedge. Phys Med Biol 1985; 30(9):985e91.

[14] Andreo P, Burns D T, Hohlfeld K, Huq M S, Kanai T, Laitano F, et al. Absorbed dose determination in external beam radiotherapy: An international Code of Practice for dosimetry based on standards of absorbed dose to water IAEA Technical Report Series No 398 IAEA. Vienna; 2000.

[15] Philips Medical Systems Division Product Data 764, (Eindoven, the Netherlands: Philips; 1983.

[16] Zwicker RD, Shahabi S, Wu A, Stemick ES. Effective wedge angles for 6-MV wedges. Med Phys 1985; 12:347e9.

[17] IBA (2013): Detectors for relative and absolute dosimetry. world wide web:http://iba-dosimetry.com/product. Retrieved on 15th March, 2015.

[18] Arya Amini, Norman Yeh, Laurie E Gaspar, Brian Kavanagh and Sana D Karam. Stereotactic Body Radiation Therapy (SBRT) for lung cancer patients previously treated with conventional radiotherapy: 2014.

[19] Purdy J. A (1996): Intensity modulated radiation therapy, Int. J Radiat oncol, Biol. Phy. (4), 845-846

[20] Weber L, Nilsson P, Ahnesjö A. Build-up cap materials for measurement of photon head-scatter factors. Phys Med Biol. 1997; 42(10):1875–86.

[21] Schmidt Ernst-Ludwig, Rittler Jiirgen, Steurer Reiner. A method for quality assurance of dynamic wedge. Strahlenther Onkol 1999; 175:39e41.

[22] Huq MS, Das IJ, Steinberg T et al: A dosimetric comparison of various multileaf collimators. Phys Med Biol, 2002; 47: N159–70

[23] Haryanto F, Fippel M, Bakai A et al: Study on the Tongue and Groove Effect of the Elekta Multileaf Collimator Using Monte Carlo Simulation and Film Dosimetry. Strahlenther Oncol, 2004; 180: 57–61 5. Szarf W, Siebers J: Biomedical particle accelerators. American Institute of Physics, 1994

[24] Van Dyk J: The modern technology of radiation oncology. Medical Physics Pub, 1999.

[25] Tailor RC, Followill DS, Hanson WF. A first order approximation of field-size and depth dependence of wedge transmission. Med Phys. 1998; 25:241–244.

[26] Arthur G. Wedge factors for rectangular fields. Australas Phys Eng Sci Med. 1994; 17:43–48.

[27] Vadash P, Bjärngard B. An equivalent-square formula for head-scatter factors. Med Phys. 1993; 20:733–734.

[28] Castellanos ME, Rosenwald JC. Evaluation of the scatter field for high-energy photon beam attenuators. Phys Med Biol. 1998; 43:277–290.

[29] Liu HH, Mackie TR, McCullough EC. Calculating dose and output factors for wedged photon radiotherapy fields using a convolution/superposition method. Med Phys. 1997; 24:1714–1728.

[30] Hounsell AR, Wilkinson JM. The variation in output of symmetric, asymmetric and irregularly shaped wedged radiotherapy fields. Phys Med Biol. 1996; 41:2155–2172.

[31] Saeed Ahmad Buzdar, M. Afzal Khan, Aalia Nazir, M. A. Gadhi, Altaf H. Nizamani, Hussain Saleem. Effect of Change in Orientation of Enhanced Dynamic Wedges on Radiotherapy Treatment Dose. Intl J. of Adv. in Res & Tech Vol 2, 2013.

[32] Anthink Hoog and Bernhard Christoph. Prediction of tumor definition for Image Guided Radiation Therapy. Thesis work at State University of New at York at Buffalo: 2011

[33] Christopher F. Njeh, Enhanced dynamic wedge output factors for Varian 2300CD and the case for a reference database. J Appl Clin Med Phys. 2015.

[34] Leavitt DD, Lee WL, Gaffney DK, Moeller JH, O'Rear JH. Dosimetric parameters of enhanced dynamic wedge for treatment planning and verification. Med Dosim. 1997; 22(3):177–83.

[35] Koken PW, Heukelom S, Cuijpers JP. On the practice of the clinical implementation of enhanced dynamic wedges. Med Dosim. 2003; 28(1):13–19.

[36] Saminathan S, Manickam R, Supe SS. Comparison of dosimetric characteristics of physical and enhanced dynamic wedges. Rep Pract Oncol Radiother. 2011; 17(1):4–12.

[37] Avadhani JS, Pradhan AS, Sankar A, Viswanathan PS. Dosimetric aspects of physical and dynamic wedge of Clinac 2100C linear accelerator. Strahlenther Onkol. 1997; 173(10):524–28.

[38] Ahmad M, Hussain A, Muhammad W, Rizvi SQ, Matiullah. Studying wedge factors and beam profiles for physical and enhanced dynamic wedges. J Med Phys. 2010; 35(1):33-41.

[39] Heukelom S, Lanson JH, Mijnheer BJ. Wedge factor constituents of high energy photon beams: Field size and depth dependence. Radiother Oncol. 1994; 30:66–73.

[40] Popescu A, Lai K, Singer K, Phillips M. Wedge factor dependence with depth, field size, and nominal distance— A general computational rule. Med Phys. 1999; 26:541–549.

[41] Arthur G. Wedge factors for rectangular fields. Australas Phys Eng Sci Med. 1994; 17:43–48

[42] Heukelom S, Lanson JH, Mijnheer BJ. Wedge factor constituents of high-energy photon beams: Head and phantom scatter dose components. Radiother Oncol. 1994; 32:73–83.

[43] Zhu TC, Bjarngard BE, Vadash P. Scattered photons from wedges in high-energy x-ray beams. Med Phys. 1995; 22:1339–1342.

[44] Palta JR, Daftari I, Suntharalingam N. Field size dependence of wedge factors. Med Phys. 1988; 15:624–626.

[45] Malhotra H., Wu V.,Wang Z., Patil S. (2012): A novel method for viginal cylinder treatment planning; a seamless transition to 3D brachytherapy. Med. Phys. Vol. 4(2); 92-100.

[46] Karabis A., Belloti P. and Baltas D.(2009): Optimization of Catheter Position and Dwell Time in Prostate HDR Brachytherapy using HIPO and Linear Programming WC in Med. Physics & Biomedical Eng., Vol. 25/I, pp. 612-615, Springer.

[47] Galvin, James M; Ezzell, Gary; Eisbrauch, Avraham; Yu, Cedric; Butler, Brian; Xiao, Ying; Rosen, Isaac; Rosenman, Julian; Sharpe, Michael; Xing, Lei; Xia, Ping; Lomax, Tony; Low, Daniel A; Palta, Jatinder (April 2004), "Implementing IMRT in clinical practice: a joint document of the American Society for Therapeutic Radiology and Oncology and the American Association of Physicists in Medicine.", Int J Radiat Oncol Biol Phys. **58** (5): 1616– 34.

[48] International Commission On Radiation Units And Measurements, (ICRU), "Prescribing, recording, and reporting photon beam therapy", International Com-mission on Radiation Units and Measurements, ICRU Report 50, ICRU, Bethesda, Maryland, U.S.A. (1993).

[49] Lahanas M, Baltas D, Giannouli S (2003) Global convergence analysis of fast multiobjective gradient-based dose optimization algorithms for high-dose- rate brachytherapy. Phys Med Biol 48:599-617.

[50] P. Hejazi, B. Hashemi, M. Shahriari, M. Eivazi, A. Kazemnejad. An Investigation on the Internal Wedge Factor Estimation for an Elekta Linac using Monte Carlo Simulation, 2009.

[51] IAEA, "Absorbed Dose Determination in External Beam Radiotherapy", Technical Reports Series No. 398, IAEA, Vienna (2000).

[52] Large field auto wedge functional description, Elekta Oncology Systems Ltd., Fleming Way, Crawley.

[53] Radiation Oncology Physics, A hand book for teachers and students, E.B Podgosak Technical Editor, (2004).

[54] D.C. Murray, P. W. Hoban, W. H. Round, I. *D.* Graham, and P. E. Metcalfe, Superposition on a Multicomputer system, , *Medical Physics,vo*\. 18, no. 3, pp. 468^173, May(1991).

[55] Dai J, Zhu Y, Ji Q , Optimizing beam weights and wedge filters with the concept of the super-omni wedge, Med Phys; 27:2757-62, (2000).

[56] Faiz. M. Khan, PHD, The physics of radiation therapy, 3rd edition, (2003).

[57] Hoban P.W. Murry D.C. Round W.H, Photon beam convolution using poly energetic energy deposition kernels, Phys. Med. Biol .39:669-685, (1994).

[58] Hoban P.W., Accounting for the variation in kerma/terma, (1995).

[59] J. V. Siebers, Monte Carlo for radiation therapy dose calculations, online: Available www.radonc.rdo.vcu.edu/AAPM, (2002).

APPENDIX

APPENDIX ONE

Table 1. A Table Showing Dose Measured with Wedge in place, Open Field Doses, And Their Computed Wedge Output Factor for 6 MV with Collimator 0°.

FIELD SIZE	WA	IN	OUT	Dw/nC	Dw/Gy	OF	OF/Gy	WOF
	15	1.792	10.23	12.022	0.649428	16.98	0.91726	0.708009
5*5	30	2.897	6.05	8.947	0.483317	16.98	0.91726	0.526914
	45	3.744	2.876	6.62	0.357612	16.98	0.91726	0.38987
	60	4.503		4.503	0.243252	16.98	0.91726	0.265194
	15	1.925	10.75	12.675	0.684704	17.85	0.964257	0.710084
10*10	30	3.114	6.353	9.467	0.511407	17.85	0.964257	0.530364
	45	4.02	3.022	7.042	0.380409	17.85	0.964257	0.39451
	60	4.838		4.838	0.261349	17.85	0.964257	0.271036
	15	2.02	11.02	13.04	0.704421	18.31	0.989106	0.712179
15*15	30	3.268	6.522	9.79	0.528856	18.31	0.989106	0.534681
	45	4.217	3.097	7.314	0.395102	18.31	0.989106	0.399454
	60	5.077		5.077	0.27426	18.31	0.989106	0.27728
	15	2.109	11.24	13.349	0.721113	18.67	1.008553	0.714997
20*20	30	3.412	6.645	10.057	0.543279	18.67	1.008553	0.538672
	45	4.399	3.162	7.561	0.408445	18.67	1.008553	0.404981
	60	5.297		5.297	0.286144	18.67	1.008553	0.283717
	15	2.156	11.35	13.506	0.729594	18.84	1.017737	0.716879
25*25	30	3.485	6.709	10.194	0.55068	18.84	1.017737	0.541083
	45	4.498	3.187	7.685	0.415144	18.84	1.017737	0.407909
	60	5.413		5.413	0.29241	18.84	1.017737	0.287314
	15	2.183	11.41	13.593	0.734294	18.95	1.023679	0.717309
30*30	30	3.532	6.743	10.275	0.555056	18.95	1.023679	0.542216
	45	4.556	3.207	7.763	0.419357	18.95	1.023679	0.409657
	60	5.483		5.483	0.296192	18.95	1.023679	0.28934
MEAN								0.482235

Table 2. A Table Showing Dose Measured with Wedge in place, Open Field Doses, And Their Computed Wedge Output Factor for 6 MV with Collimator 90°.

FIELD SIZE	WA	IN	OUT	Dw/nC	Dw/Gy	OF	OF/Gy	WOF
	15	1.76	10.22	11.98	0.64716	16.96	0.916179	0.706368
5*5	30	2.848	6.04	8.888	0.48013	16.96	0.916179	0.524057
	45	3.672	2.871	6.543	0.353453	16.96	0.916179	0.38579
	60	4.419		4.419	0.238714	16.96	0.916179	0.260554
	15	1.892	10.75	12.642	0.682921	17.84	0.963717	0.708632
10*10	30	3.06	6.355	9.415	0.508598	17.84	0.963717	0.527747
	45	3.947	3.019	6.966	0.376303	17.84	0.963717	0.390471
	60	4.75		4.75	0.256595	17.84	0.963717	0.266256
	15	1.985	11.02	13.005	0.70253	18.3	0.988566	0.710656
15*15	30	3.211	6.512	9.723	0.525236	18.3	0.988566	0.531311
	45	4.143	3.095	7.238	0.390997	18.3	0.988566	0.395519
	60	4.985		4.985	0.26929	18.3	0.988566	0.272404
	15	2.074	11.24	13.314	0.719222	18.66	1.008013	0.713505
20*20	30	3.354	6.644	9.998	0.540092	18.66	1.008013	0.535798
	45	4.326	3.056	7.382	0.398776	18.66	1.008013	0.395606
	60	5.206		5.206	0.281228	18.66	1.008013	0.278992
	15	2.121	11.34	13.461	0.727163	18.83	1.017197	0.71487
25*25	30	3.43	6.706	10.136	0.547547	18.83	1.017197	0.53829
	45	4.424	3.187	7.611	0.411146	18.83	1.017197	0.404195
	60	5.324		5.324	0.287602	18.83	1.017197	0.28274
	15	2.151	11.41	13.561	0.732565	18.96	1.024219	0.715243
30*30	30	3.476	6.749	10.225	0.552355	18.96	1.024219	0.539293
	45	4.485	3.204	7.689	0.41536	18.96	1.024219	0.405538
	60	5.397		5.397	0.291546	18.96	1.024219	0.284652

Table 3. A Table Showing Dose Measured With Wedge in place, Open Field Doses, And Their Computed Wedge Output Factor For 15 MV With Collimator 0°.

FIELD SIZE	WA	IN	OUT	Dw/nC	Dw/Gy	OF	OF/Gy	WOF
	15	1.807	10.16	11.967	0.646457	16.74	0.904295	0.714875
5*5	30	2.946	6.076	9.022	0.487368	16.74	0.904295	0.538949
	45	3.831	2.904	6.735	0.363825	16.74	0.904295	0.40233
	60	4.656		4.656	0.251517	16.74	0.904295	0.278136
	15	1.984	10.93	12.914	0.697614	17.9	0.966958	0.721453
10*10	30	3.239	6.537	9.776	0.5281	17.9	0.966958	0.546145
	45	4.214	3.126	7.34	0.396507	17.9	0.966958	0.410056
	60	5.394		5.394	0.291384	17.9	0.966958	0.301341
	15	2.119	11.39	13.509	0.729756	18.63	1.006393	0.725121
15*15	30	3.454	6.798	10.252	0.553813	18.63	1.006393	0.550295
	45	4.493	3.25	7.743	0.418277	18.63	1.006393	0.41562
	60	5.441		5.441	0.293923	18.63	1.006393	0.292056
	15	2.237	11.73	13.967	0.754497	19.18	1.036104	0.728206
20*20	30	3.651	7.01	10.661	0.575907	19.18	1.036104	0.555839
	45	4.752	3	8.098	0.437454	19.18	1.036104	0.422211
	60	5.752		5.752	0.310723	19.18	1.036104	0.299896
	15	2.305	11.88	14.185	0.766274	19.44	1.050149	0.729681
25*25	30	3.759	7.104	10.863	0.586819	19.44	1.050149	0.558796
	45	4.889	3.393	8.282	0.447394	19.44	1.050149	0.426029
	60	5.917		5.917	0.319636	19.44	1.050149	0.304372
	15	2.344	11.98	14.324	0.773782	19.61	1.059332	0.730444
30*30	30	3.827	7.161	10.988	0.593572	19.61	1.059332	0.560326
	45	4.976	3.424	8.4	0.453768	19.61	1.059332	0.428353
	60	6.025		6.025	0.325471	19.61	1.059332	0.307241

Table 4. A Table Showing Dose Measured with Wedge in place, Open Field Doses, And Their Computed Wedge Output Factor for 15 MV with Collimator 90°.

FIELD SIZE	WA	IN	OUT	Dw/nC	Dw/Gy	OF	OF/Gy	WOF
	15	1.774	10.16	11.934	0.644675	16.75	0.904835	0.712478
5*5	30	2.895	6.079	8.974	0.484775	16.75	0.904835	0.535761
	45	3.764	2.906	6.67	0.360313	16.75	0.904835	0.398209
	60	6.691		6.691	0.361448	16.75	0.904835	0.399463
	15	1.953	10.94	12.893	0.69648	17.89	0.966418	0.720682
10*10	30	3.186	6.544	9.73	0.525615	17.89	0.966418	0.543879
	45	4.143	3.122	7.265	0.392455	17.89	0.966418	0.406093
	60	5.014		5.014	0.270856	17.89	0.966418	0.280268
	15	2.085	11.38	13.465	0.727379	18.63	1.006393	0.722759
15*15	30	3.4	7.167	10.567	0.570829	18.63	1.006393	0.567203
	45	4.421	3.25	7.671	0.414387	18.63	1.006393	0.411755
	60	5.355		5.355	0.289277	18.63	1.006393	0.28744
	15	2.204	11.73	13.934	0.752715	19.18	1.036104	0.726486
20*20	30	3.597	7.013	10.61	0.573152	19.18	1.036104	0.55318
	45	4.676	3.349	8.025	0.433511	19.18	1.036104	0.418405
	60	5.661		5.661	0.305807	19.18	1.036104	0.295151
	15	2.267	11.87	14.137	0.763681	19.42	1.049068	0.727961
25*25	30	3.7	7.102	10.802	0.583524	19.42	1.049068	0.556231
	45	4.814	3.39	8.204	0.44318	19.42	1.049068	0.422451
	60	5.828		5.828	0.314829	19.42	1.049068	0.300103
	15	2.311	11.98	14.291	0.772	19.61	1.059332	0.728761
30*30	30	3.771	7.162	10.933	0.590601	19.61	1.059332	0.557522
	45	4.902	3.421	8.323	0.449608	19.61	1.059332	0.424426
	60	5.938		5.938	0.320771	19.61	1.059332	0.302805

Table 5. A Table Showing Field Sizes, Wedge Angles, Wedge Output Factors, Mean, Difference, Percentage Difference, Standard Deviation, Percent Standard Deviation and Coefficient of Variation for 6 MV Photon Energy (Collimator 0 And 90).

FIELD SIZES	WA	WOF 0	WOF 90	MEAN	DIFFERENCE	% DIFFERENCE	STD	% STD	COV
	15	0.708009	0.706368	0.707189	0.001641498	0.232116037	0.001160715	0.116071459	0.164130824
5*5	30	0.526914	0.524057	0.525485	0.002857413	0.543766431	0.002020496	0.202049591	0.384500931
	45	0.38987	0.38579	0.38783	0.004080341	1.052094649	0.002885237	0.288523712	0.743943261
	60	0.265194	0.260554	0.262874	0.004640101	1.765140632	0.003281047	0.328104689	1.248142911
	15	0.710084	0.708632	0.709358	0.001451747	0.204656364	0.00102654	0.102653988	0.144713903
10*10	30	0.530364	0.527747	0.529055	0.002617509	0.494751387	0.001850858	0.185085828	0.349842061
	45	0.39451	0.390471	0.39249	0.004038952	1.02905769	0.00285597	0.285597028	0.727653671
	60	0.271036	0.266256	0.268646	0.004780809	1.779594339	0.003380543	0.338054259	1.258363225
	15	0.712179	0.710656	0.711417	0.001523399	0.214135794	0.001077206	0.107720603	0.151416872
15*15	30	0.534681	0.531311	0.532996	0.003369027	0.632092383	0.002382262	0.238226187	0.44695681
	45	0.399454	0.395519	0.397486	0.003934725	0.989901491	0.00278227	0.27822705	0.699966057
	60	0.27728	0.272404	0.274842	0.004875803	1.774036842	0.003447713	0.344771349	1.254433481
	15	0.714997	0.713505	0.714251	0.001492499	0.20895996	0.001055356	0.105535599	0.147757005
20*20	30	0.538672	0.535798	0.537235	0.002873166	0.534806159	0.002031635	0.203163538	0.378165062
	45	0.404981	0.395606	0.400293	0.00937568	2.342201899	0.006629607	0.662960686	1.656186845
	60	0.283717	0.278992	0.281355	0.004724696	1.679265922	0.003340865	0.334086461	1.187420321
	15	0.716879	0.71487	0.715874	0.002009092	0.280648717	0.001420643	0.142064287	0.198448611
25*25	30	0.541083	0.53829	0.539686	0.00279284	0.517493087	0.001974836	0.197483591	0.365922871
	45	0.407909	0.404195	0.406052	0.003713272	0.91448175	0.00262568	0.262567986	0.646636246
	60	0.287314	0.28274	0.285027	0.004573917	1.604729642	0.003234248	0.323424775	1.134715212
	15	0.717309	0.715243	0.716276	0.002066091	0.288449155	0.001460947	0.146094702	0.203964353
30*30	30	0.542216	0.539293	0.540755	0.00292311	0.540561059	0.002066951	0.206695083	0.38223439
	45	0.409657	0.405538	0.407597	0.004119017	1.010560067	0.002912585	0.291258514	0.714573876
	60	0.28934	0.284652	0.286996	0.004688471	1.633635475	0.003315249	0.33152494	1.155154723

Table 6. A Table Showing Field Sizes, Wedge Angles, Wedge Output Factors, Mean, Difference, Percentage Difference, Standard Deviation, Percent Standard Deviation and Coefficient of Variation for 6 MV Photon Energy (Collimator 0 And 90) From Treatment Planning System.

FIELD SIZE	WA	TPS 0	TPS 90	MEAN	DIFFERENCE	% DIFFERENCE	STD	% STD	COV
	15	0.705263158	0.705263158	0.705263158	0	0	0	0	0
5*5	30	0.526315789	0.526315789	0.526315789	0	0	0	0	0
	45	0.389473684	0.389473684	0.389473684	0	0	0	0	0
	60	0.263157895	0.263157895	0.263157895	0	0	0	0	0
	15	0.717171717	0.717171717	0.717171717	0	0	0	0	0
10*10	30	0.525252525	0.525252525	0.525252525	0	0	0	0	0
	45	0.393939394	0.393939394	0.393939394	0	0	0	0	0
	60	0.272727273	0.272727273	0.272727273	0	0	0	0	0
	15	0.715686275	0.715686275	0.715686275	0	0	0	0	0
15*15	30	0.529411765	0.539215686	0.534313725	-0.009803922	-1.834862385	0.006932419	0.693241942	1.297443635
	45	0.401960784	0.401960784	0.401960784	0	0	0	0	0
	60	0.274509804	0.274509804	0.274509804	0	0	0	0	0
	15	0.711538462	0.721153846	0.716346154	-0.009615385	-1.342281879	0.006799104	0.679910367	0.949136619
20*20	30	0.538461538	0.538461538	0.538461538	0	0	0	0	0
	45	0.394230769	0.403846154	0.399038462	-0.009615385	-2.409638554	0.006799104	0.679910367	1.703871762
	60	0.278846154	0.278846154	0.278846154	0	0	0	0	0
	15	0.714285714	0.721153846	0.71771978	-0.006868132	-0.956937799	0.004856503	0.485650262	0.676657207
25*25	30	0.533333333	0.538461538	0.535897436	-0.005128205	-0.956937799	0.003626189	0.362618862	0.676657207
	45	0.40952381	0.403846154	0.406684982	0.005677656	1.396081964	0.004014709	0.401470883	0.987179023
	60	0.285714286	0.278846154	0.28228022	0.006868132	2.433090024	0.004856503	0.485650262	1.720454455
	15	0.714285714	0.721153846	0.71771978	-0.006868132	-0.956937799	0.004856503	0.485650262	0.676657207
30*30	30	0.533333333	0.538461538	0.535897436	-0.005128205	-0.956937799	0.003626189	0.362618862	0.676657207
	45	0.40952381	0.413461538	0.411492674	-0.003937729	-0.956937799	0.002784395	0.278439483	0.676657207
	60	0.285714286	0.288461538	0.287087912	-0.002747253	-0.956937799	0.001942601	0.194260105	0.676657207

Table 7. A Table Showing Field Sizes, Wedge Angles, Wedge Output Factors, Mean, Difference, Percentage Difference, Standard Deviation, Percent Standard Deviation and Coefficient of Variation for 15 MV Photon Energy (Collimator 0 And 90).

FIELD SIZES	WA	WOF	WOF	MEAN	DIFFERENCE	% DIFFERENCE	STD	% STD	COV
	15	0.713445	0.711053	0.712249	0.002392146	0.335858254	0.001691503	0.169150276	0.237487649
5*5	30	0.537871	0.53469	0.53628	0.003181057	0.593170725	0.002249347	0.224934708	0.419435042
	45	0.401525	0.397413	0.399469	0.004112552	1.029505221	0.002908014	0.290801361	0.727970123
	60	0.27758	0.398664	0.338122	-0.121083833	-35.81070988	0.085619199	8.561919932	25.3219958
	15	0.72001	0.719241	0.719625	0.000769028	0.106865035	0.000543785	0.054378464	0.075564991
10*10	30	0.545053	0.542792	0.543922	0.002261457	0.415768492	0.001599092	0.159909176	0.29399272
	45	0.409236	0.405281	0.407258	0.003955151	0.971165395	0.002796714	0.279671374	0.686717636
	60	0.300738	0.279708	0.290223	0.021030331	7.246267717	0.01487069	1.487068956	5.123885041
	15	0.723671	0.721313	0.722492	0.002357059	0.326240083	0.001666692	0.166669205	0.230686575
15*15	30	0.549195	0.566069	0.557632	-0.016874396	-3.026081944	0.011932	1.193199994	2.139763063
	45	0.414789	0.410932	0.41286	0.003857005	0.934215648	0.002727314	0.272731427	0.66059022
	60	0.291472	0.286865	0.289168	0.004606978	1.59318266	0.003257625	0.325762538	1.126550263
	15	0.72675	0.725033	0.725892	0.001717101	0.236550661	0.001214174	0.121417387	0.167266577
20*20	30	0.554728	0.552074	0.553401	0.002653702	0.479526115	0.001876451	0.187645052	0.339076168
	45	0.421366	0.417568	0.419467	0.003798436	0.905538671	0.0026859	0.268589976	0.640312535
	60	0.299296	0.294561	0.296928	0.004735036	1.594672742	0.003348176	0.334817642	1.127603909
	15	0.728222	0.726505	0.727363	0.001716764	0.236025711	0.001213936	0.121393579	0.166895381
25*25	30	0.557679	0.555118	0.556398	0.002560475	0.460187299	0.001810529	0.181052929	0.32540156
	45	0.425177	0.421606	0.423391	0.00357057	0.843325876	0.002524774	0.25247741	0.596321446
	60	0.303764	0.299503	0.301633	0.004260902	1.412610428	0.003012913	0.301291304	0.998866413
	15	0.728983	0.727303	0.728143	0.001679449	0.230648261	0.00118755	0.118754996	0.16309295
30*30	30	0.559206	0.556407	0.557806	0.002799082	0.501801925	0.00197925	0.197924993	0.354827544
	45	0.427496	0.423577	0.425537	0.003918715	0.920887401	0.00277095	0.277094991	0.651165726
	60	0.306627	0.302199	0.304413	0.004427639	1.454484661	0.003130814	0.313081353	1.028475967

Table 8. A Table Showing Field Sizes, Wedge Angles, Wedge Output Factors, Mean, Difference, Percentage Difference, Standard Deviation, Percent Standard Deviation and Coefficient of Variation for 15 MV Photon Energy (Collimator 0 And 90) From Treatment Planning System.

FIELD SIZE	WA	WOF TPS	WOF TPS	MEAN	DIFFEREN	% DIFFERE	STD	% STD	COV
	15	0.717391	0.717391	0.717391	0	0	0	0	0
5*5	30	0.554348	0.554348	0.554348	0	0	0	0	0
	45	0.413043	0.413043	0.413043	0	0	0	0	0
	60	0.282609	0.402174	0.342391	-0.11957	-34.9206	0.084545	8.454538	24.69262
	15	0.72449	0.721649	0.72307	0.00284	0.392813	0.002008	0.20084	0.277761
10*10	30	0.55102	0.556701	0.553861	-0.00568	-1.02564	0.004017	0.401681	0.725238
	45	0.408163	0.412371	0.410267	-0.00421	-1.02564	0.002975	0.297541	0.725238
	60	0.408163	0.28866	0.348412	0.119503	34.29952	0.084502	8.450172	24.25342
	15	0.732673	0.732673	0.732673	0	0	0	0	0
15*15	30	0.554455	0.554455	0.554455	0	0	0	0	0
	45	0.425743	0.425743	0.425743	0	0	0	0	0
	60	0.29703	0.29703	0.29703	0	0	0	0	0
	15	0.735294	0.72549	0.730392	0.009804	1.342282	0.006932	0.693242	0.949137
20*20	30	0.54902	0.54902	0.54902	0	0	0	0	0
	45	0.421569	0.421569	0.421569	0	0	0	0	0
	60	0.303922	0.303922	0.303922	0	0	0	0	0
	15	0.728155	0.728155	0.728155	0	0	0	0	0
25*25	30	0.563107	0.563107	0.563107	0	0	0	0	0
	45	0.427184	0.427184	0.427184	0	0	0	0	0
	60	0.300971	0.300971	0.300971	0	0	0	0	0
	15	0.728155	0.728155	0.728155	0	0	0	0	0
30*30	30	0.563107	0.563107	0.563107	0	0	0	0	0
	45	0.427184	0.427184	0.427184	0	0	0	0	0
	60	0.300971	0.300971	0.300971	0	0	0	0	0

APPENDIX TWO

Table 1. A table of Values showing, Difference, Percentage difference, Mean, Standard Deviation, % Standard Deviation and COV for 6 MV, 45° Wedge.

45° WEDGE								
FIELD SIZE	Cal. MWOF	Mea. MWOF	Difference	% Difference	Mean	Stdev	% Stdev	COV
5×5	0.389474	0.387830	0.0016434	0.4219590	0.388652	0.001162	0.116207	0.299001
10×10	0.393939	0.392490	0.0014491	0.3678398	0.393215	0.001025	0.102464	0.260581
15×15	0.401961	0.397487	0.0044743	1.1131176	0.399724	0.003164	0.316381	0.791498
20×20	0.399038	0.400293	-0.001255	-0.3144940	0.399666	0.000887	0.088738	0.222032
25×25	0.406685	0.406052	0.0006329	0.1556273	0.406369	0.000448	0.044754	0.110131
30×30	0.411493	0.407598	0.0038952	0.9466002	0.409545	0.002754	0.275432	0.672531

Table 2. A table of Values showing, Difference, Percentage difference, Mean, Standard Deviation, % Standard Deviation and COV for 15 MV, 15° Wedge.

15° WEDGE								
FIELD SIZE	Cal. WOF	Mea. WOF	Difference	% Difference	Mean	Stdev	% Stdev	COV
5×5	0.717391	0.712249	0.005143	0.716844	0.71482	0.003636	0.363635	0.508708
10×10	0.72307	0.719625	0.003445	0.476378	0.721347	0.002436	0.243566	0.337654
15×15	0.732673	0.722492	0.010181	1.389605	0.727583	0.007199	0.719924	0.989474
20×20	0.730392	0.725892	0.004501	0.616197	0.728142	0.003182	0.318244	0.437064
25×25	0.728155	0.727363	0.000792	0.10877	0.727759	0.00056	0.056004	0.076954
30×30	0.728155	0.728143	1.23E-05	0.001689	0.728149	8.7E-06	0.00087	0.001195

Table 3. A table of Values showing, Difference, Percentage difference, Mean, Standard Deviation, % Standard Deviation and COV for 15 MV, 30° Wedge.

30° WEDGE								
FIELD SIZE	Cal. WOF	Mea. WOF	Difference	% Difference	Mean	Stdev	% Stdev	COV
5×5	0.554348	0.53628	0.018068	3.259258	0.545314	0.012776	1.277574	2.342823
10×10	0.553861	0.543922	0.009938	1.794402	0.548891	0.007028	0.702757	1.280321
15×15	0.554455	0.557632	-0.00318	-0.57288	0.556044	0.002246	0.224604	0.403933
20×20	0.54902	0.553401	-0.00438	-0.79802	0.55121	0.003098	0.309803	0.562042
25×25	0.563107	0.556398	0.006708	1.191307	0.559753	0.004744	0.474351	0.847429
30×30	0.563107	0.557806	0.005301	0.941318	0.560456	0.003748	0.374811	0.66876

Table 4. A table of Values showing, Difference, Percentage difference, Mean, Standard Deviation, % Standard Deviation and COV for 15 MV, 45° Wedge.

45 WEDGE								
FIELD SIZE	Cal. WOF	Mea. WOF	Difference	% Difference	Mean	Stdev	% Stdev	COV
5×5	0.413043	0.399469	0.013575	3.286498	0.406256	0.009599	0.959874	2.36273
10×10	0.410267	0.407258	0.003009	0.73343	0.408763	0.002128	0.21277	0.520522
15×15	0.425743	0.41286	0.012882	3.025854	0.419301	0.009109	0.91092	2.17247
20×20	0.421569	0.419467	0.002102	0.498526	0.420518	0.001486	0.148608	0.353392
25×25	0.427184	0.423391	0.003793	0.887907	0.425288	0.002682	0.268206	0.630645
30×30	0.427184	0.425537	0.001648	0.385699	0.426361	0.001165	0.116506	0.273258

Table 5. A table of Values showing, Difference, Percentage difference, Mean, Standard Deviation, % Standard Deviation and COV for 15 MV, 60° Wedge.

60° WEDGE								
FIELD SIZE	Cal. WOF	Mea. WOF	Difference	% Difference	Mean	Stdev	% Stdev	COV
5×5	0.342391	0.338122	0.004269	1.246953	0.340257	0.003019	0.301896	0.887261
10×10	0.348412	0.290223	0.058189	16.70111	0.319317	0.041146	4.114555	12.88548
15×15	0.29703	0.289168	0.007861	2.646698	0.293099	0.005559	0.555891	1.896597
20×20	0.303922	0.296928	0.006993	2.300973	0.300425	0.004945	0.494491	1.64597
25×25	0.300971	0.301633	-0.00066	-0.22007	0.301302	0.000468	0.046836	0.155445
30×30	0.300971	0.304413	-0.00344	-1.14364	0.302692	0.002434	0.243388	0.804079

APPENDIX THREE

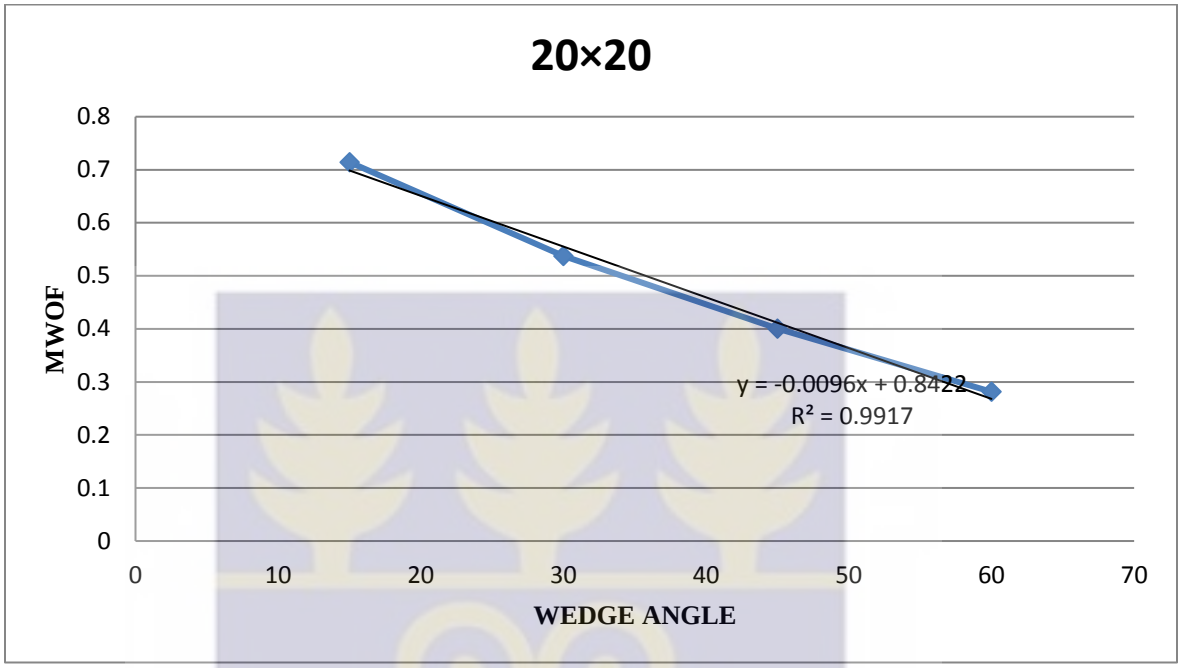

Fig 1. A Graph of Motorized Wedge Output Factor and Wedge Angle for 20×20 cm^2 6 MV.

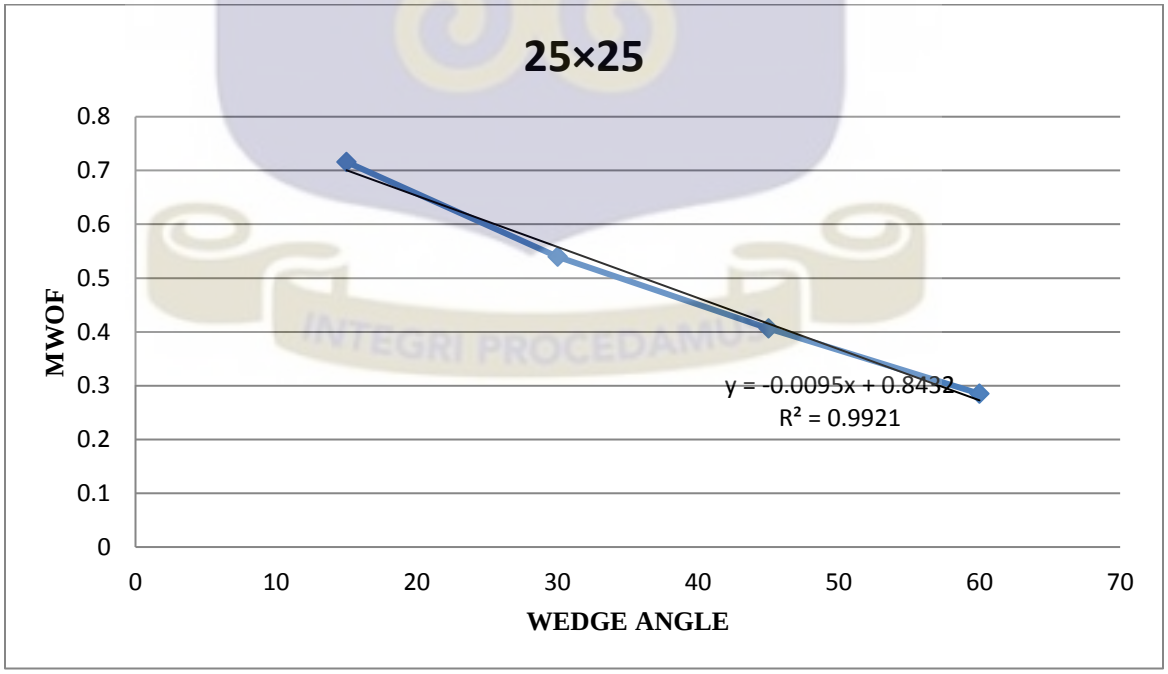

Fig 2. A Graph of Motorized Wedge Output Factor and Wedge Angle for 25×25 cm^2 6 MV.

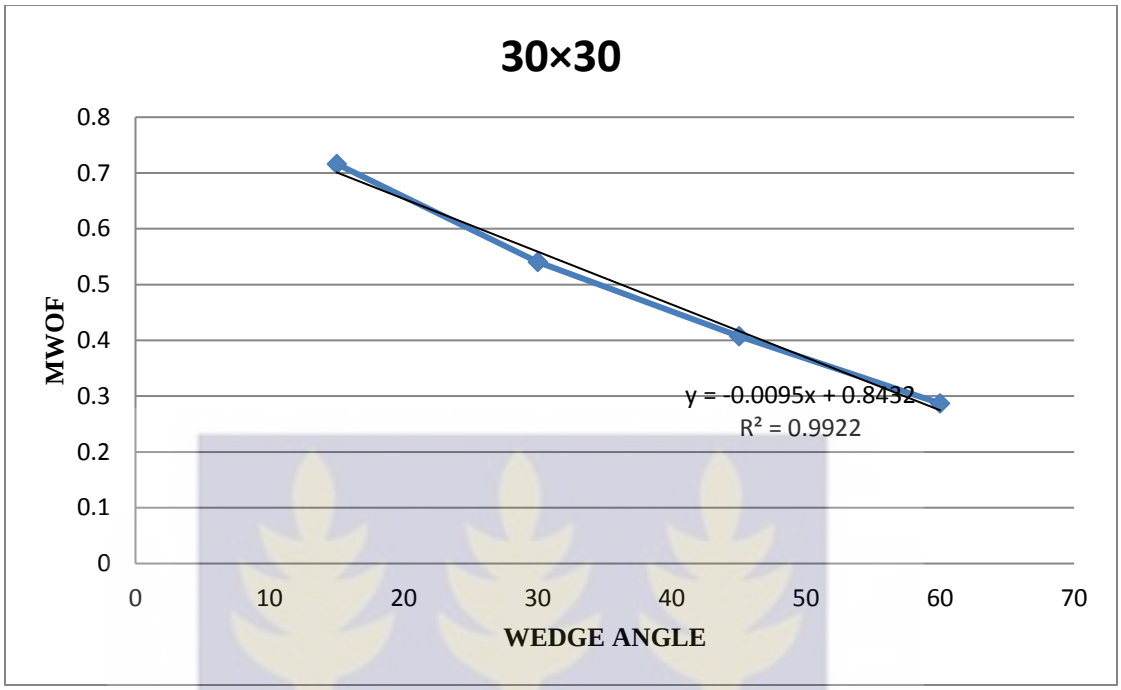

Fig 3. A Graph of Motorized Wedge Output Factor and Wedge Angle for 30×30 cm^2 6 MV.

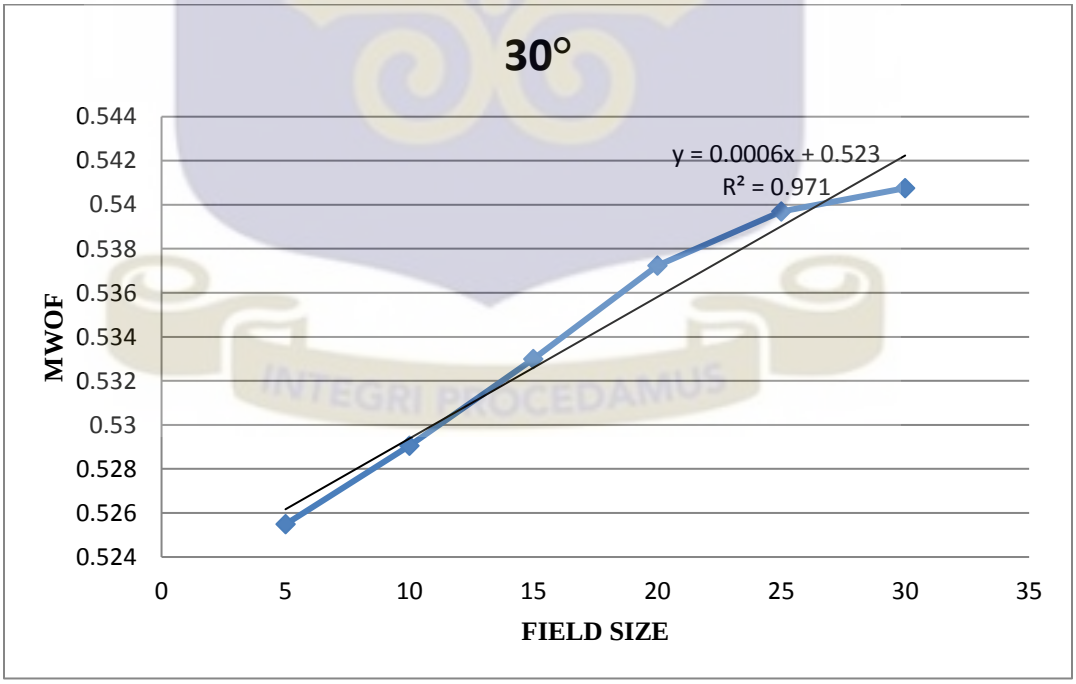

Fig 4. A Graph of Motorized Wedge Output Factor and Field Size for 30°, 6 MV

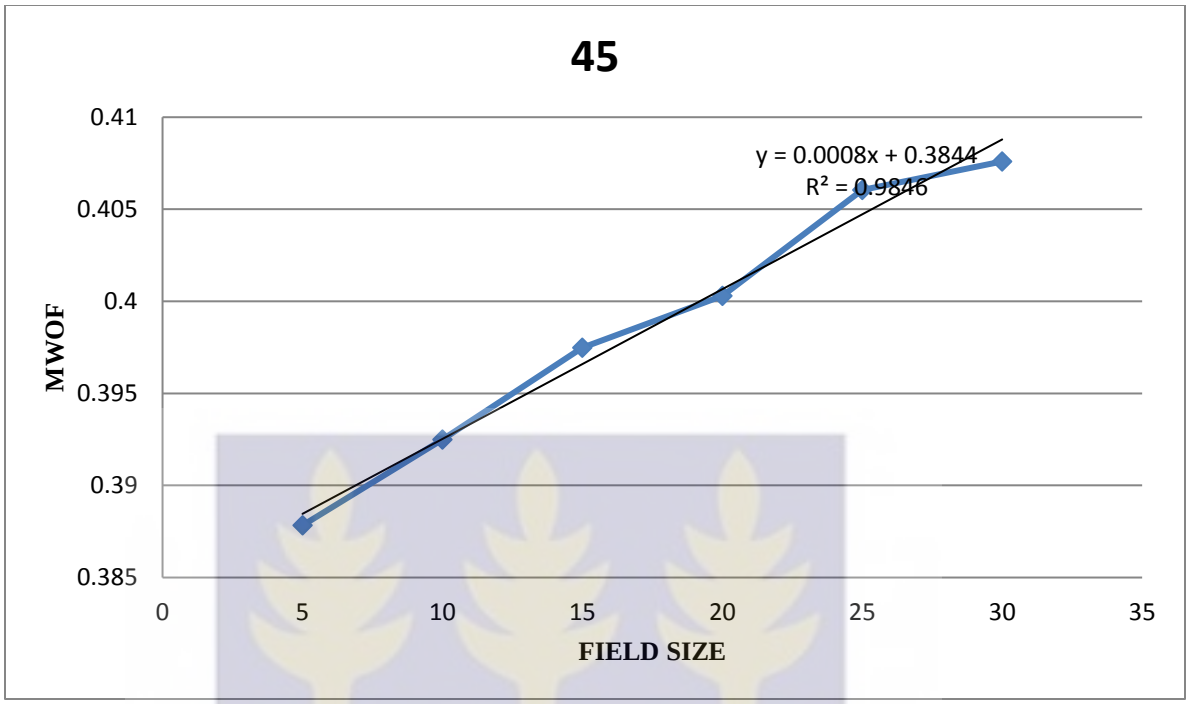

Fig 5. A Graph of Motorized Wedge Output Factor and Field Size for 45°, 6 MV.

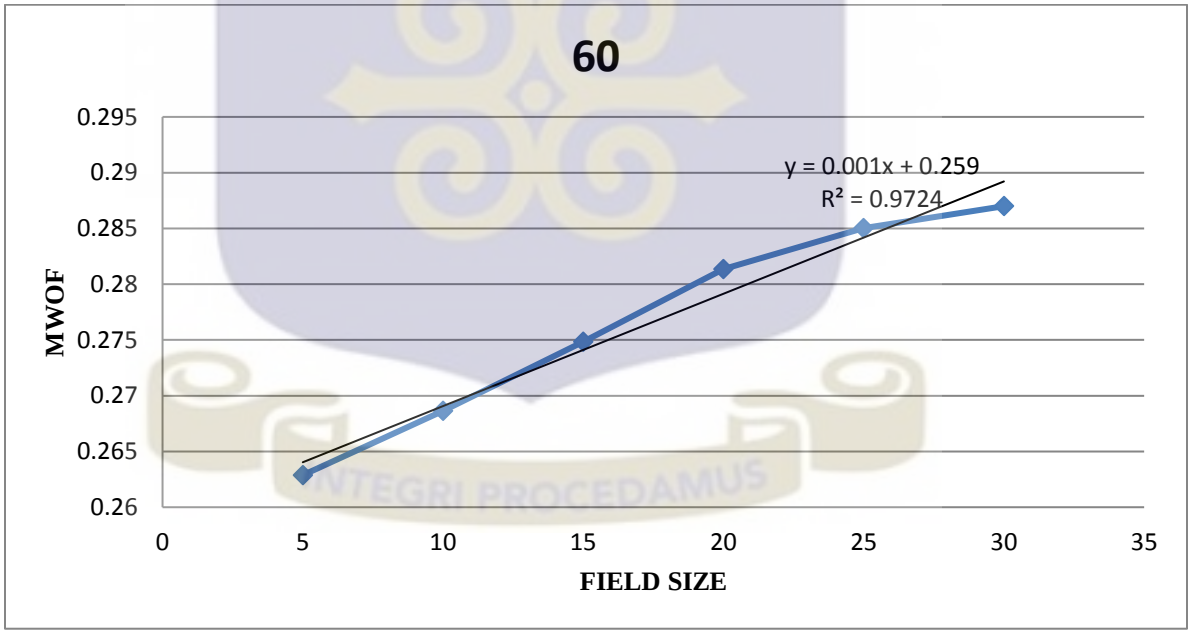

Fig 6. A Graph of Motorized Wedge Output Factor and Field Size for 60°, 6 MV

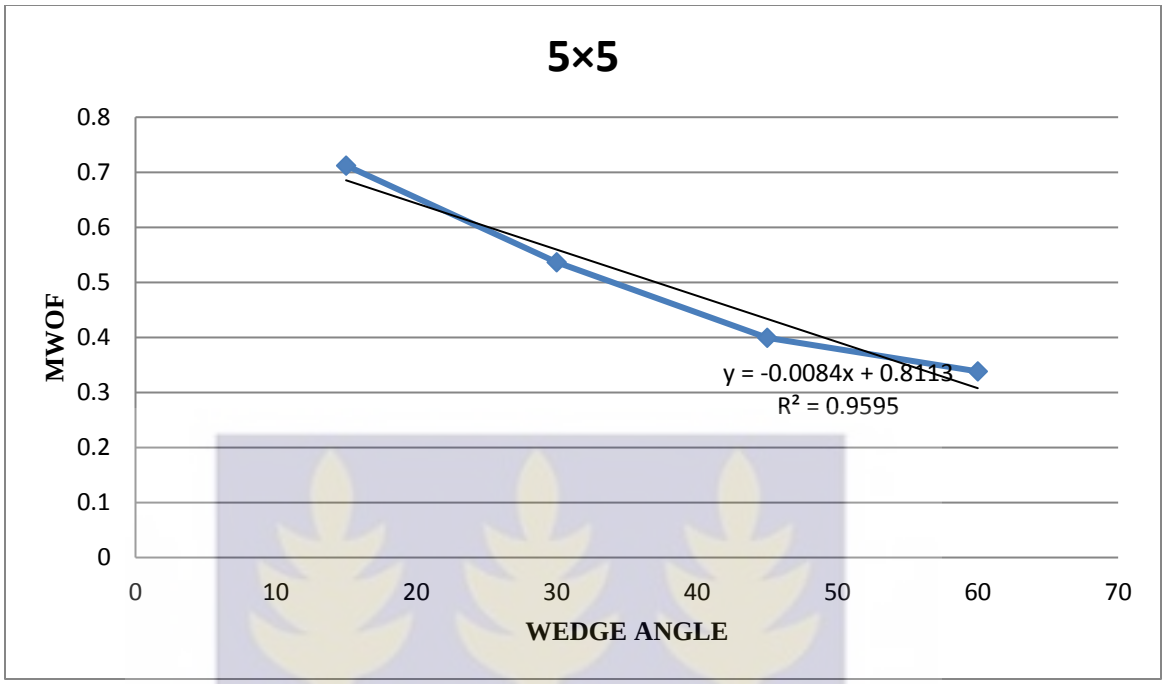

Fig 7. A Graph of Motorized Wedge Output Factor and Wedge Angle for 5×5 cm^2, 15 MV.

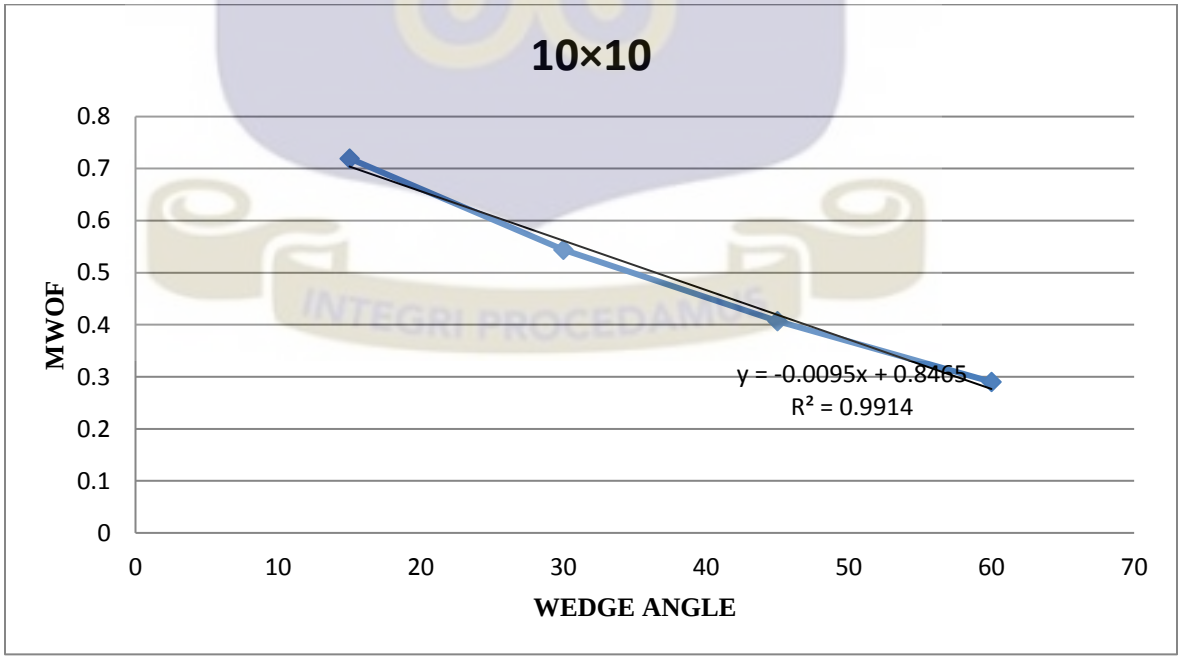

Fig 8. A Graph of Motorized Wedge Output Factor and Wedge Angle for 10×10 cm^2, 15 MV.

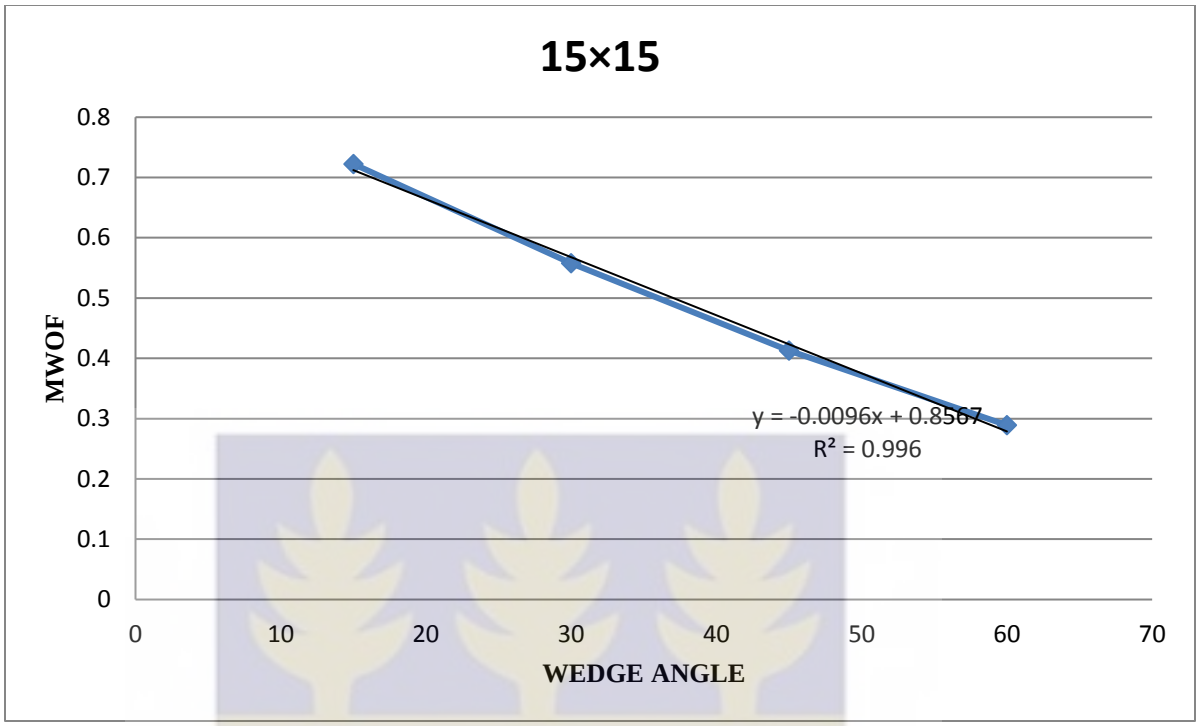

Fig 9. A Graph of Motorized Wedge Output Factor and Wedge Angle for 15×15 cm^2, 15 MV.

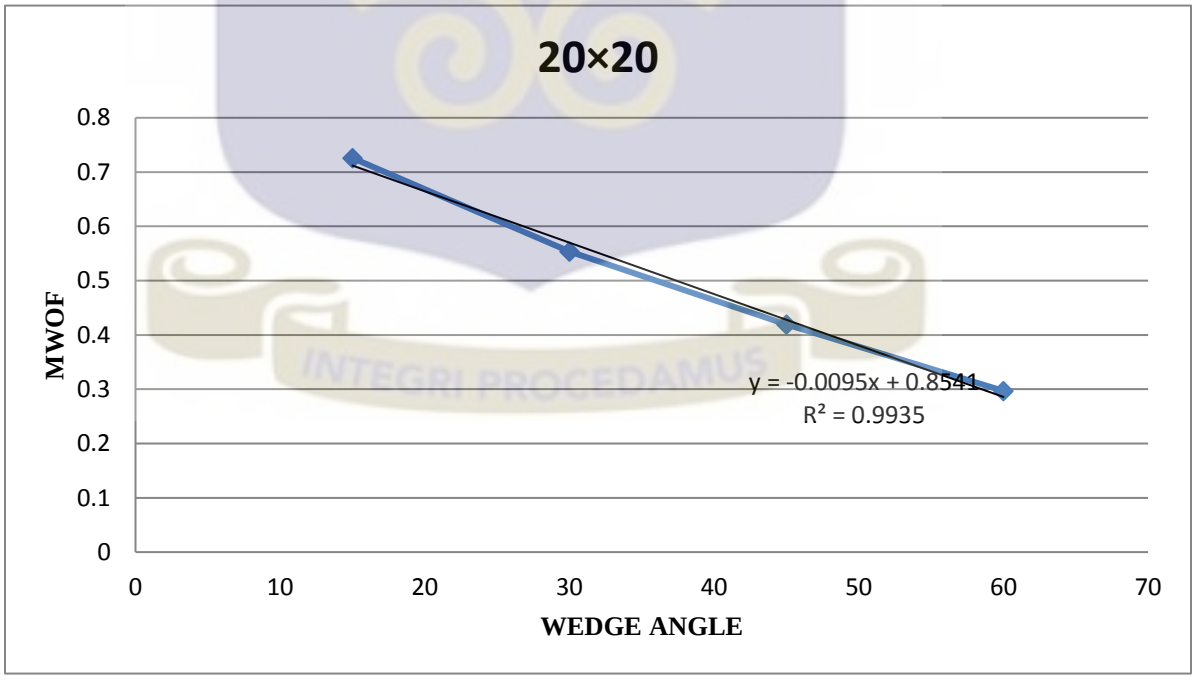

Fig 10 A Graph of Motorized Wedge Output Factor and Wedge Angle for 20×20 cm^2, 15 MV.

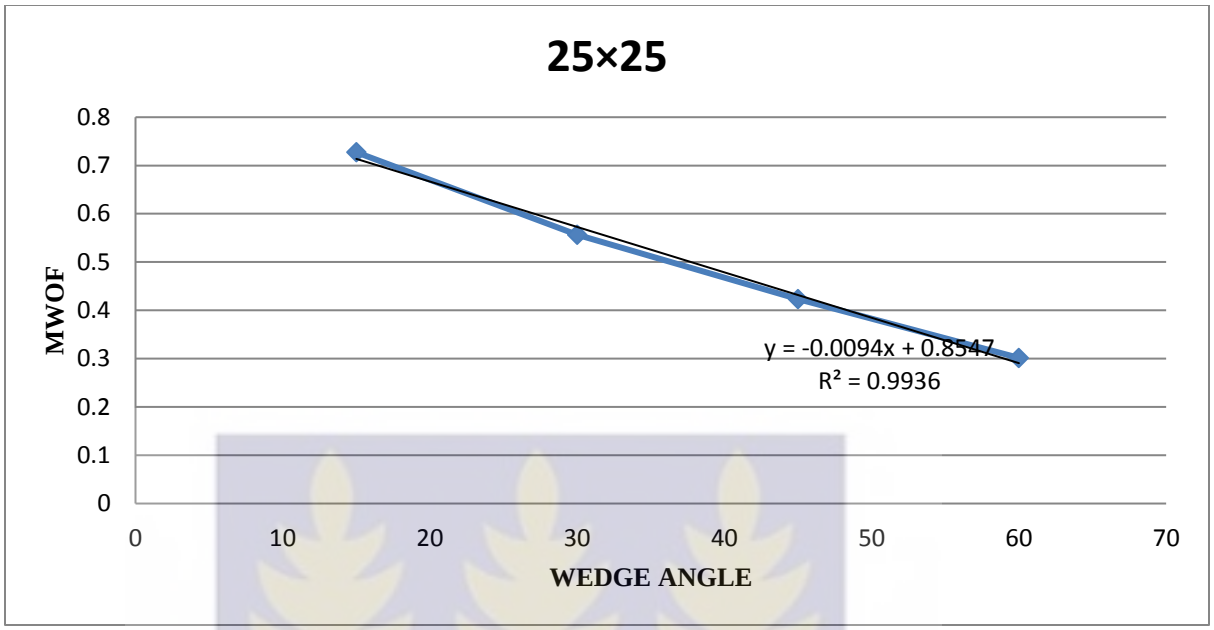

Fig 11. A Graph of Motorized Wedge Output Factor and Wedge Angle for 25×25 cm^2, 15 MV.

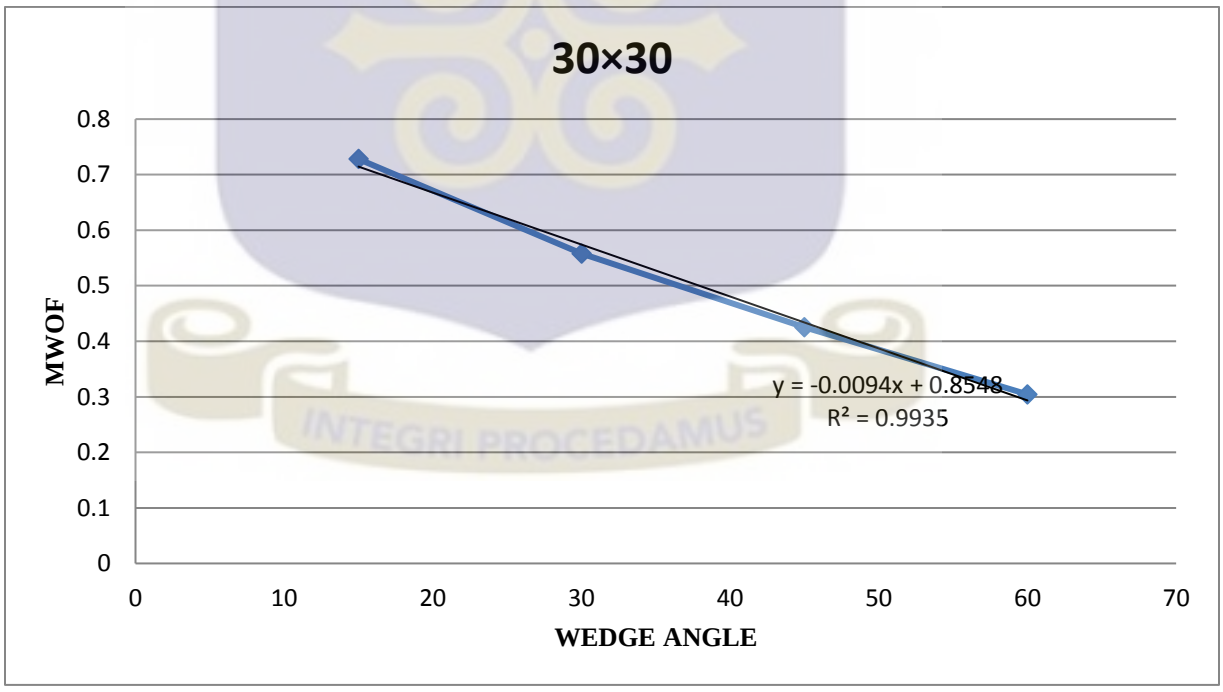

Fig 12. A Graph of Motorized Wedge Output Factor and Wedge Angle FOR 30×30 cm^2, 15 MV.

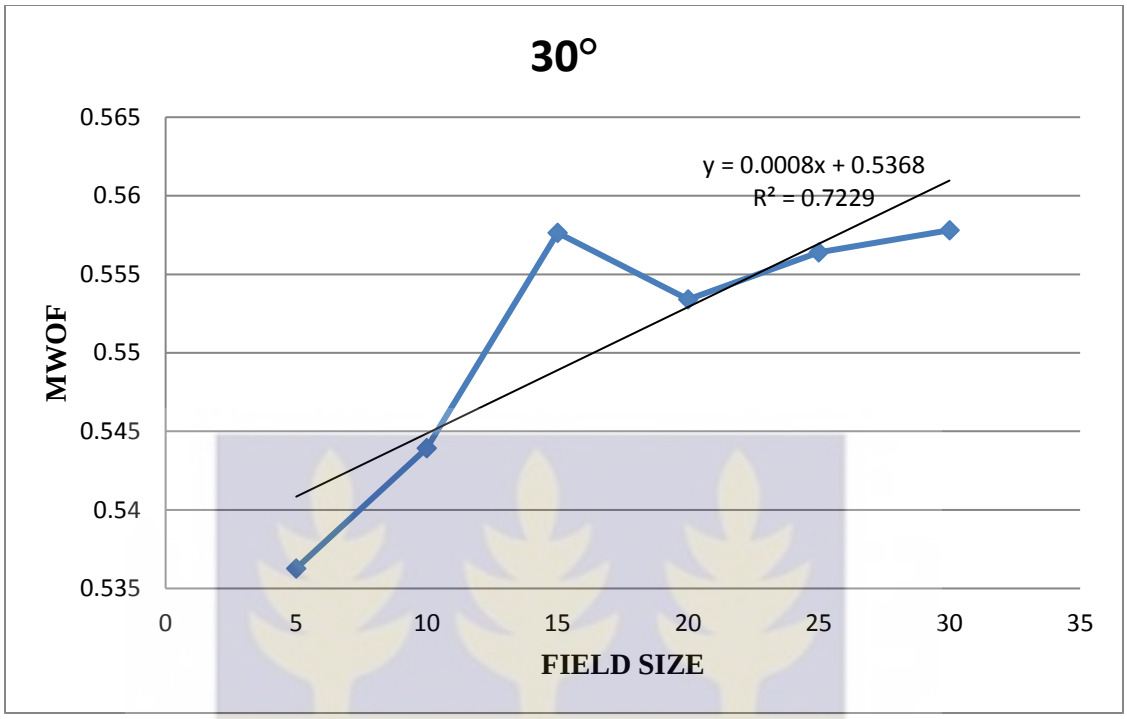

Fig 13 A Graph of Motorized Wedge Output Factor and Field Size for 30°, 15 MV

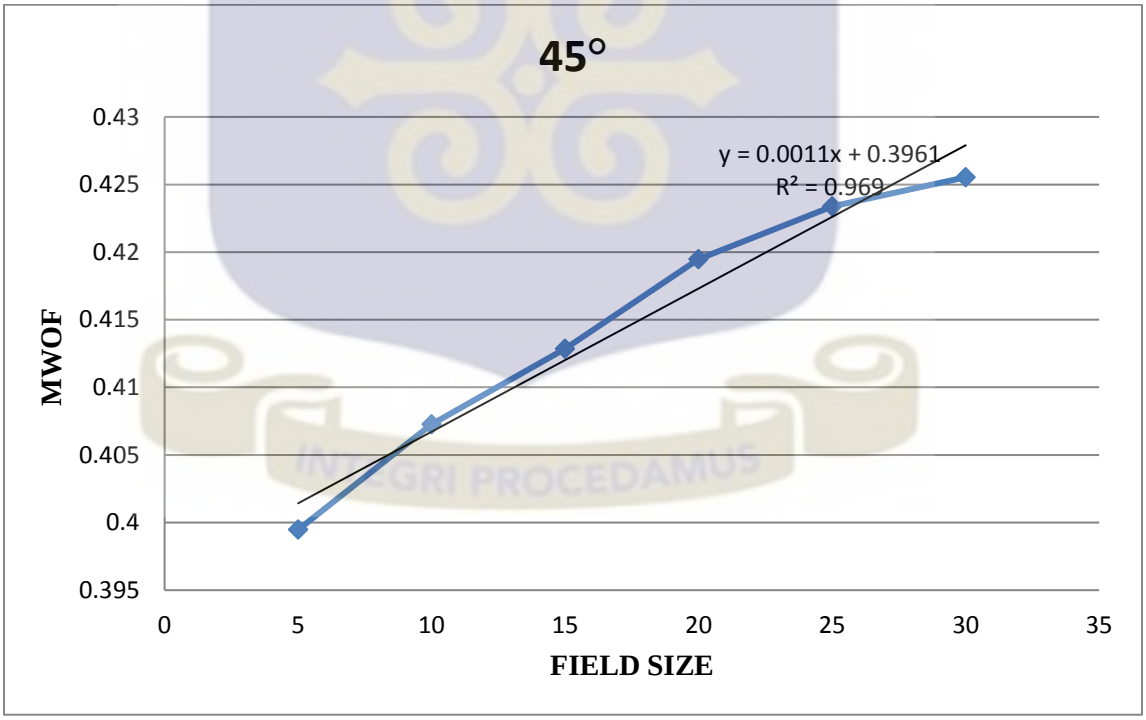

Fig 14. A Graph of Motorized Wedge Output Factor and Field Size for 45°, 15 MV.

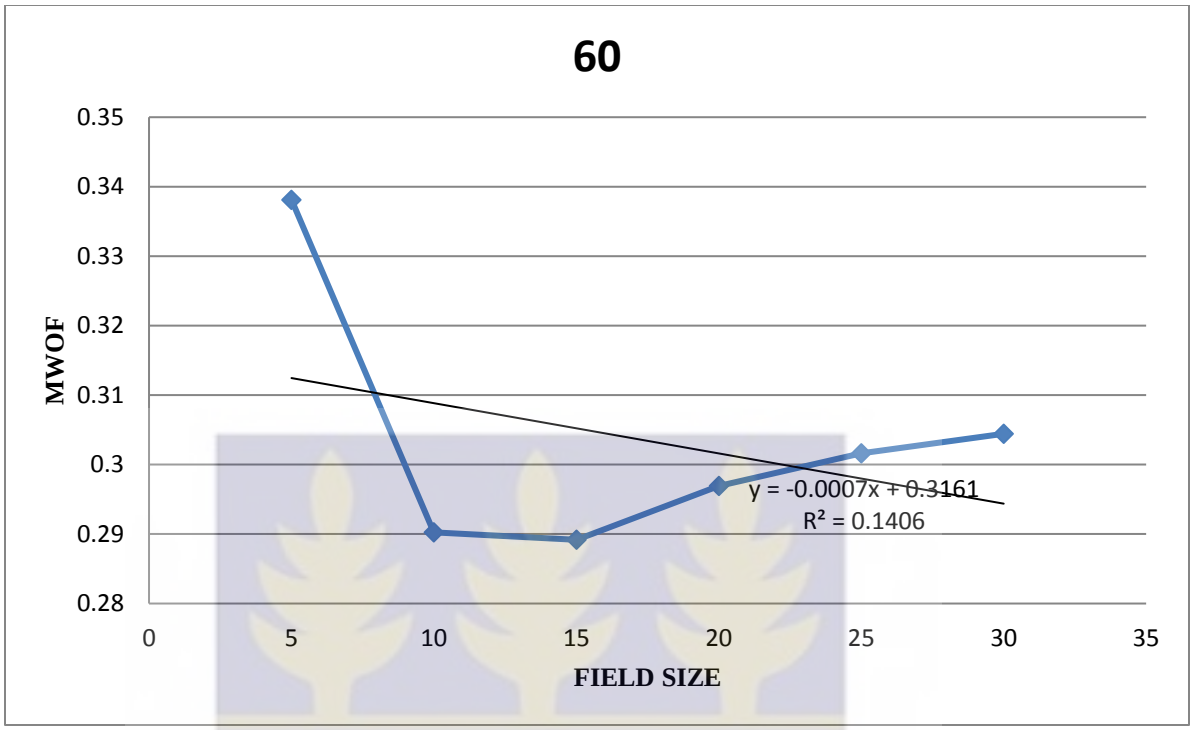

Fig 15. A Graph of Motorized Wedge Output Factor and Field Size for 60°, 15 MV.

APPENDIX FOUR

DOSE CALCULATIONS AND THEIR CORRESPOMDING MOTORISED WEDGE OUTPUT FACTOR

1. $D_{WQ} = M_Q \bullet N_{DWQ} \bullet k_{QQ.}$

$D_{WQ} = 12.022\ nC \times (5.402 \times 10^7 \frac{Gy}{C}) \times 1.00$

$D_{WQ} = 0.649428\ Gy$

$MWOF = \frac{Dw(a,b,w)}{Dc(a,b,o)}$

$MWOF = \frac{0.649428}{0.91726}$

$MWOF = 0.708009$

2. $D_{WQ} = 8.947\ nC \times (5.402 \times 10^7 \frac{Gy}{C}) \times 1.00$

$D_{WQ} = 0.483317\ Gy$

$MWOF = \frac{0.483317}{0.91726}$

$MWOF = 0.526914$

3. $D_{WQ} = 6{,}62\ nC \times (5.402 \times 10^7 \frac{Gy}{C}) \times 1.00$

$D_{WQ} = 0.357612\ Gy$

$MWOF = \frac{0.357612}{0.91726}$

$MWOF = 0.38987$

4. $D_{WQ} = 4.503\ nC \times (5.402 \times 10^7 \frac{Gy}{C}) \times 1.00$

$D_{WQ} = 0.243252\ Gy$

$MWOF = \frac{0.243252}{0.91726}$

$MWOF = 0.265194$

5. $D_{WQ} = 12{,}675\ nC \times (5.402 \times 10^7 \frac{Gy}{C}) \times 1.00$

$D_{WQ} = 0.684704\ Gy$

$MWOF = \frac{0.684704}{0.91726}$

$MWOF = 0.710084$